molecular pharmaceutics

articles

Boosting Oncolytic Adenovirus Potency with Magnetic Nanoparticles and Magnetic Force

Nittaya Tresilwised,[†,‡] Pimolpan Pithayanukul,[*,‡] Olga Mykhaylyk,[†] Per Sonne Holm,[†] Regina Holzmüller,[†] Martina Anton,[†] Stefan Thalhammer,[§] Denis Adigüzel,[§] Markus Döblinger,[||] and Christian Plank[*,†]

Institute of Experimental Oncology and Therapy Research, Technische Universität München, Munich 81675, Germany, Department of Pharmacy, Faculty of Pharmacy, Mahidol University, Bangkok 10400, Thailand, Helmholtz Zentrum München, AG NanoAnalytics, Neuherberg 85764, Germany, and Department of Chemistry and Biochemistry, Ludwig-Maximilians-Universität München, Munich 81377, Germany

Received July 25, 2009; Revised Manuscript Received June 2, 2010; Accepted June 15, 2010

Abstract: Oncolytic adenoviruses rank among the most promising innovative agents in cancer therapy. We examined the potential of boosting the efficacy of the oncolytic adenovirus dl520 by associating it with magnetic nanoparticles and magnetic-field-guided infection in multidrug-resistant (MDR) cancer cells in vitro and upon intratumoral injection in vivo. The virus was complexed by self-assembly with core−shell nanoparticles having a magnetite core of about 10 nm and stabilized by a shell containing 68 mass % lithium 3-[2-(perfluoroalkyl)ethylthio]propionate) and 32 mass % 25 kDa branched polyethylenimine. Optimized virus binding, sufficiently stable in 50% fetal calf serum, was found at nanoparticle-to-virus ratios of 5 fg of Fe per physical virus particle (VP) and above. As estimated from magnetophoretic mobility measurements, 3,600 to 4,500 magnetite nanocrystallites were associated per virus particle. Ultrastructural analysis by electron and atomic force microscopy showed structurally intact viruses surrounded by magnetic particles that occasionally bridged several virus particles. Viral uptake into cells at a given virus dose was enhanced 10-fold compared to nonmagnetic virus when infections were carried out under the influence of a magnetic field. Increased virus internalization resulted in a 10-fold enhancement of the oncolytic potency in terms of the dose required for killing 50% of the target cells (IC_{50} value) and an enhancement of 4 orders of magnitude in virus progeny formation at equal input virus doses compared to nonmagnetic viruses. Furthermore, the full oncolytic effect developed within two days postinfection compared with six days in a nonmagnetic virus as a reference. Plotting target cell viability versus internalized virus particles for magnetic and nonmagnetic virus showed that the inherent oncolytic productivity of the virus remained unchanged upon association with magnetic nanoparticles. Hence, we conclude that the mechanism of boosting the oncolytic effect by magnetic force is mainly due to the improved internalization of magnetic virus complexes resulting in potentiated virus progeny formation. Upon intratumoral injection and application of a gradient magnetic field in a murine xenograft model, magnetic virus complexes exhibited a stronger oncolytic effect than adenovirus alone. We propose that this approach would be useful during in vivo administration to tumor-feeding blood vessels to boost the efficacy of the primary

10.1021/mp100123t
Published on Web 06/15/2010

infection cycle within the tumor. For systemic application, further modification of magnetic adenovirus complexes for shielding and retargeting of the whole magnetic virus complex entity is needed.

Keywords: Oncolytic adenovirus; magnetic nanoparticles; magnetofection; magnetic drug targeting

Introduction

Oncolytic virotherapy holds substantial promise of yielding potent curative treatments for cancer. Oncolytic viruses are designed, mostly by molecular biological methods, to preferentially replicate in cancer cells and destroy them as part of the replication cycle. Among the virus types that are being explored for oncolytic virotherapy, adenovirus (Ad) has advanced the furthest in clinical development and is currently approved for clinical use in China. Truly encouraging results have been obtained upon localized administration of adenovirus into solid tumors in combination with chemotherapy in patients.[1−3] On the other hand, experts in the field have pointed out that, upon intravenous (iv) administration, this virus lacks efficacy in comparison to other virus species that currently are in clinical trials.[1−3] Adenovirus does not have an inherent tropism for preferentially infecting tumor cells. Rather, the infectivity of this virus in tumor cells can be limited, particularly if the cells lack apical coxsackie virus and adenovirus receptor, CAR.[3−6] Although there is more and more evidence to indicate that CAR is not the only primary Ad receptor in vivo,[7,8] achieving efficacy for oncolytic adenovirus upon systemic administration is an unresolved challenge. Most of the virotherapy clinical trials were done by local or locoregional administration.[9] Current approaches aim to equip oncolytic adenoviruses with targeting and shielding moieties for the delivery phase and to arm them with further antitumoral functionality.[10] This can be achieved by molecular-biological and chemical means. For example, coating the virus with hydrophilic polymers with tagged targeting ligands can be exploited to overcome a systemic antiviral immune response (for example, by neutralizing antibodies and complement) and to retarget the virus to chosen receptors.[11] Another strategy was to use carrier cells (T cells, endothelial cells or mesenchymal stem cells) infected with an oncolytic virus to chaperone the virus to the sites of tumor growth.[12−14] Numerous approaches of arming oncolytic viruses, which are also excellent gene vectors, have been described.[10] For example, equipping oncolytic viruses with cytokine

* Corresponding authors. P.P.: Department of Pharmacy, Faculty of Pharmacy, Mahidol University, 447 Sri-Ayudthaya Road, Payatai, Bangkok 10400, Thailand; tel/fax, +66 26 44 86 94; e-mail, pypph@mahidol.ac.th. C.P.: Institute of Experimental Oncology and Therapy Research, Technische Universität München, Munich 81675, Germany; tel, +49-89-4140-4453; fax, +49-89-4140-4476; e-mail, plank@lrz.tu-muenchen.de.

† Technische Universität Munich.

‡ Mahidol University.

§ AG NanoAnalytics.

|| Ludwig-Maximilians-Universität Munich.

(1) Liu, T. C.; Galanis, E.; Kirn, D. Clinical trial results with oncolytic virotherapy: a century of promise, a decade of progress. *Nat. Clin. Pract. Oncol.* **2007**, *4* (2), 101–17.

(2) Campbell, S. A.; Gromeier, M. Oncolytic viruses for cancer therapy II. Cell-internal factors for conditional growth in neoplastic cells. *Onkologie* **2005**, *28* (4), 209–15.

(3) Campbell, S. A.; Gromeier, M. Oncolytic viruses for cancer therapy I. Cell-external factors: virus entry and receptor interaction. *Onkologie* **2005**, *28* (3), 144–9.

(4) Strauss, R.; Lieber, A. Anatomical and physical barriers to tumor targeting with oncolytic adenoviruses in vivo. *Curr. Opin. Mol. Ther.* **2009**, *11* (5), 513–22.

(5) Walters, R. W.; Grunst, T.; Bergelson, J. M.; Finberg, R. W.; Welsh, M. J.; Zabner, J. Basolateral localization of fiber receptors limits adenovirus infection from the apical surface of airway epithelia. *J. Biol. Chem.* **1999**, *274* (15), 10219–26.

(6) Yamamoto, M.; Curiel, D. T. Current issues and future directions of oncolytic adenoviruses. *Mol. Ther.* **2010**, *18* (2), 243–50.

(7) Arnberg, N. Adenovirus receptors: implications for tropism, treatment and targeting. *Rev. Med. Virol.* **2009**, *19* (3), 165–78.

(8) Smith, T. A.; Idamakanti, N.; Marshall-Neff, J.; Rollence, M. L.; Wright, P.; Kaloss, M.; King, L.; Mech, C.; Dinges, L.; Iverson, W. O.; Sherer, A. D.; Markovits, J. E.; Lyons, R. M.; Kaleko, M.; Stevenson, S. C. Receptor interactions involved in adenoviral-mediated gene delivery after systemic administration in non-human primates. *Hum. Gene Ther.* **2003**, *14* (17), 1595–604.

(9) Liu, T. C.; Kirn, D. Gene therapy progress and prospects cancer: oncolytic viruses. *Gene Ther.* **2008**, *15* (12), 877–84.

(10) Cattaneo, R.; Miest, T.; Shashkova, E. V.; Barry, M. A. Reprogrammed viruses as cancer therapeutics: targeted, armed and shielded. *Nat. Rev. Microbiol.* **2008**, *6* (7), 529–40.

(11) Morrison, J.; Briggs, S. S.; Green, N. K.; Thoma, C.; Fisher, K. D.; Kehoe, S.; Seymour, L. W. Cetuximab retargeting of adenovirus via the epidermal growth factor receptor for treatment of intraperitoneal ovarian cancer. *Hum. Gene Ther.* **2009**, *20* (3), 239–51.

(12) Hakkarainen, T.; Sarkioja, M.; Lehenkari, P.; Miettinen, S.; Ylikomi, T.; Suuronen, R.; Desmond, R. A.; Kanerva, A.; Hemminki, A. Human mesenchymal stem cells lack tumor tropism but enhance the antitumor activity of oncolytic adenoviruses in orthotopic lung and breast tumors. *Hum. Gene Ther.* **2007**, *18* (7), 627–41.

(13) Iankov, I. D.; Blechacz, B.; Liu, C.; Schmeckpeper, J. D.; Tarara, J. E.; Federspiel, M. J.; Caplice, N.; Russell, S. J. Infected cell carriers: a new strategy for systemic delivery of oncolytic measles viruses in cancer virotherapy. *Mol. Ther.* **2007**, *15* (1), 114–22.

(14) Power, A. T.; Bell, J. C. Cell-based delivery of oncolytic viruses: a new strategic alliance for a biological strike against cancer. *Mol. Ther.* **2007**, *15* (4), 660–5.

genes,[15] prodrug convertase genes, or genes of apoptosis-inducing or angiogenesis-inhibiting[16] factors has been exploited to upgrade their arsenal beyond merely oncolytic potency.

No matter how sophisticated these approaches are, the first and essential step remains the primary infection cycle and its efficacy. We and others have shown in the context of gene delivery that this first step can be enhanced by enforcing target cell contact with gradient magnetic fields acting on gene vectors that are associated with magnetic nanoparticles.[17−30] In particular, this method, which is also known as magnetofection,[31] can be used to overcome the CAR dependence of adenoviral infection[17,26,28,32] and to localize gene delivery. Despite the many reports on magnetically enhanced infection, little is known about whether or how this concept can be exploited to enhance the oncolytic potency of replicating viruses. Therefore, as a first step toward the magnetic targeting of oncolytic adenovirus, we asked whether one could magnetically trigger infection and enhance oncolysis with a tumor-specific oncolytic adenovirus in multidrug-resistant (MDR) and CAR-deficient tumor cells in vitro. Specifically, we are interested in how physicochemical characteristics of iron oxide magnetic nanoparticles and their viral complexes correlate with the infectious and oncolytic potential of virus associated with magnetic nanoparticles in target and nontarget cells. For our studies, we chose the adenovirus dl520, which does not replicate in normal cells.[33,34] This virus is rendered cancer-specific by deletion of the trans-activation domain CR3 of the adenoviral E1A13S protein. This deletion causes antitumor activity in drug-resistant cells expressing nuclear transcription factor Y-box binding protein (YB-1).[35,36]

In this study, we quantified virus binding to well-characterized magnetic nanoparticles (MNPs), we estimated the number of MNPs associated with one virus particle from a simple photometric magnetophoretic mobility assay, and

(15) Huang, J. H.; Zhang, S. N.; Choi, K. J.; Choi, I. K.; Kim, J. H.; Lee, M.; Kim, H.; Yun, C. O. Therapeutic and tumor-specific immunity induced by combination of dendritic cells and oncolytic adenovirus expressing IL-12 and 4−1BBL. *Mol. Ther.* **2010**, *18* (2), 264–74.

(16) Yoo, J. Y.; Kim, J. H.; Kwon, Y. G.; Kim, E. C.; Kim, N. K.; Choi, H. J.; Yun, C. O. VEGF-specific short hairpin RNA-expressing oncolytic adenovirus elicits potent inhibition of angiogenesis and tumor growth. *Mol. Ther.* **2007**, *15* (2), 295–302.

(17) Bhattarai, S. R.; Kim, S. Y.; Jang, K. Y.; Lee, K. C.; Yi, H. K.; Lee, D. Y.; Kim, H. Y.; Hwang, P. H. N-hexanoyl chitosan-stabilized magnetic nanoparticles: enhancement of adenoviral-mediated gene expression both in vitro and in vivo. *Nanomedicine* **2008**, *4* (2), 146–54.

(18) Bhattarai, S. R.; Kim, S. Y.; Jang, K. Y.; Lee, K. C.; Yi, H. K.; Lee, D. Y.; Kim, H. Y.; Hwang, P. H. Laboratory formulated magnetic nanoparticles for enhancement of viral gene expression in suspension cell line. *J. Virol. Methods* **2008**, *147* (2), 213–8.

(19) Chan, L.; Nesbeth, D.; Mackey, T.; Galea-Lauri, J.; Gaken, J.; Martin, F.; Collins, M.; Mufti, G.; Farzaneh, F.; Darling, D. Conjugation of lentivirus to paramagnetic particles via nonviral proteins allows efficient concentration and infection of primary acute myeloid leukemia cells. *J. Virol.* **2005**, *79* (20), 13190–4.

(20) Chorny, M.; Fishbein, I.; Alferiev, I.; Levy, R. J. Magnetically responsive biodegradable nanoparticles enhance adenoviral gene transfer in cultured smooth muscle and endothelial cells. *Mol. Pharmaceutics* **2009**, *6* (5), 1380–7.

(21) Hofmann, A.; Wenzel, D.; Becher, U. M.; Freitag, D. F.; Klein, A. M.; Eberbeck, D.; Schulte, M.; Zimmermann, K.; Bergemann, C.; Gleich, B.; Roell, W.; Weyh, T.; Trahms, L.; Nickenig, G.; Fleischmann, B. K.; Pfeifer, A. Combined targeting of lentiviral vectors and positioning of transduced cells by magnetic nanoparticles. *Proc. Natl. Acad. Sci. U.S.A.* **2009**, *106* (1), 44–9.

(22) Hughes, C.; Galea-Lauri, J.; Farzaneh, F.; Darling, D. Streptavidin paramagnetic particles provide a choice of three affinity-based capture and magnetic concentration strategies for retroviral vectors. *Mol. Ther.* **2001**, *3* (4), 623–30.

(23) Mah, C.; Fraites, T. J., Jr.; Zolotukhin, I.; Song, S.; Flotte, T. R.; Dobson, J.; Batich, C.; Byrne, B. J. Improved method of recombinant AAV2 delivery for systemic targeted gene therapy. *Mol. Ther.* **2002**, *6* (1), 106–12.

(24) Morizono, K.; Xie, Y.; Helguera, G.; Daniels, T. R.; Lane, T. F.; Penichet, M. L.; Chen, I. S. A versatile targeting system with lentiviral vectors bearing the biotin-adaptor peptide. *J. Gene Med.* **2009**, *11* (8), 655–63.

(25) Nesbeth, D.; Williams, S. L.; Chan, L.; Brain, T.; Slater, N. K.; Farzaneh, F.; Darling, D. Metabolic biotinylation of lentiviral pseudotypes for scalable paramagnetic microparticle-dependent manipulation. *Mol. Ther.* **2006**, *13* (4), 814–22.

(26) Pandori, M.; Hobson, D.; Sano, T. Adenovirus-microbead conjugates possess enhanced infectivity: a new strategy for localized gene delivery. *Virology* **2002**, *299* (2), 204–12.

(27) Raty, J. K.; Airenne, K. J.; Marttila, A. T.; Marjomaki, V.; Hytonen, V. P.; Lehtolainen, P.; Laitinen, O. H.; Mahonen, A. J.; Kulomaa, M. S.; Yla-Herttuala, S. Enhanced gene delivery by avidin-displaying baculovirus. *Mol. Ther.* **2004**, *9* (2), 282–91.

(28) Scherer, F.; Anton, M.; Schillinger, U.; Henke, J.; Bergemann, C.; Kruger, A.; Gansbacher, B.; Plank, C. Magnetofection: enhancing and targeting gene delivery by magnetic force in vitro and in vivo. *Gene Ther.* **2002**, *9* (2), 102–9.

(29) Tai, M. F.; Chi, K. M.; Lau, K. H. W.; Baylink, D. J.; Chen, S. T. Generation of magnetic retroviral vectors with magnetic nanoparticles. *Rev. Adv. Mater. Sci.* **2003**, *5*, 319–23.

(30) Wang, X.; Mani, P.; Sarkar, D. P.; Roy-Chowdhury, N.; Roy-Chowdhury, J. Ex vivo gene transfer into hepatocytes. *Methods Mol. Biol.* **2009**, *481*, 117–40.

(31) Plank, C.; Anton, M.; Rudolph, C.; Rosenecker, J.; Krotz, F. Enhancing and targeting nucleic acid delivery by magnetic force. *Expert Opin. Biol. Ther.* **2003**, *3* (5), 745–58.

(32) Kamei, K.; Mukai, Y.; Kojima, H.; Yoshikawa, T.; Yoshikawa, M.; Kiyohara, G.; Yamamoto, T. A.; Yoshioka, Y.; Okada, N.; Seino, S.; Nakagawa, S. Direct cell entry of gold/iron-oxide magnetic nanoparticles in adenovirus mediated gene delivery. *Biomaterials* **2009**, *30* (9), 1809–14.

(33) Haley, K. P.; Overhauser, J.; Babiss, L. E.; Ginsberg, H. S.; Jones, N. C. Transformation properties of type 5 adenovirus mutants that differentially express the E1A gene products. *Proc. Natl. Acad. Sci. U.S.A.* **1984**, *81* (18), 5734–8.

(34) Wong, H. K.; Ziff, E. B. Complementary functions of E1a conserved region 1 cooperate with conserved region 3 to activate adenovirus serotype 5 early promoters. *J. Virol.* **1994**, *68* (8), 4910–20.

(35) Holm, P. S.; Bergmann, S.; Jurchott, K.; Lage, H.; Brand, K.; Ladhoff, A.; Mantwill, K.; Curiel, D. T.; Dobbelstein, M.; Dietel, M.; Gansbacher, B.; Royer, H. D. YB-1 relocates to the nucleus in adenovirus-infected cells and facilitates viral replication by inducing E2 gene expression through the E2 late promoter. *J. Biol. Chem.* **2002**, *277* (12), 10427–34.

we showed that this estimate is in agreement with ultrastructural analysis by high resolution electron (TEM) and atomic force microscopy (AFM). Furthermore, we established oncolytic dose−response relationships based on the MNP/virus ratios in both infection-resistant, replication-supportive chemoresistant 181RDB target cells and infection-permissive, replication-restrictive parental HeLa cells, which serve as a model for nontarget cells. Magnetofecting Ad520 did not alter the inherent oncolytic potential of the virus; rather, it boosted virus uptake in both cell types. The enhancement of virus internalization led to an early onset of virus replication and lowered the IC_{50} of the virus 1 order of magnitude in 181RDB cells. Suitable fine-tuning of the iron-to-virus ratio left the model nontarget HeLa parental cells largely unaffected. In a pilot experiment, we injected magnetic Ad520 complexes intratumorally in mouse tumor xenografts from human pancreatic carcinoma cells and revealed an oncolytic effect superior to that of adenovirus alone. These findings lead us to propose that magnetic guidance of viral infection can be a suitable tool in oncolytic virotherapy for localizing and reducing the virus dose required for achieving lytic action. This may in the end improve the efficacy, safety and cost-effectiveness of adenoviral oncolytic virotherapy.

Experimental Section

Cell Lines. The MDR human pancreatic carcinoma cell line EPP85-181RDB, referred to as 181RDB cells, and 181RDB cells stably expressing firefly luciferase (181RDB-fLuc) were cultured in Leibovitz's L-15 medium (Bio Whittaker) supplemented with 10% FCS, 2 mM L-glutamine, 6.25 mg/L fetuin, 2.5 mg/L transferrin, 0.5 g/L glucose, 1.1 g/L $NaHCO_3$, 1% minimal essential vitamins, 100 units/mL penicillin, and 100 μg/mL streptomycin,[37] further referred to as cell culture medium. The cells stably expressing firefly luciferase were generated by transducing 181RDB cells with a lentivirus encoding firefly luciferase as described in the Supporting Information. To ensure P-glycoprotein expression and nuclear localization of YB-1, cells were treated with 250 ng/mL daunorubicin every two weeks. Human embryonic kidney cells (293 cells) and human cervical cancer HeLa parental cells (HeLa-P) were maintained in Dulbecco's modified Eagle medium (DMEM) with 10% FCS and 2 mM L-glutamine. All cell lines were grown at 37 °C in a humidified atmosphere of 5% CO_2.

Magnetic Nanoparticles. Core/shell type iron oxide MNPs (PEI-Mag2) with a surface coating consisting of a fluorinated surfactant (ZONYL FSA or lithium 3-[2-(perfluoroalkyl)ethylthio]propionate) combined with 25 kDa branched polyethylenimine ($PEI\text{-}25_{Br}$) were synthesized by precipitation of Fe(II)/Fe(III) hydroxide from aqueous salt solution and transformation into magnetite in an oxygen-free atmosphere with immediate spontaneous adsorption of the shell components, as recently described.[38,39] The nanoparticle concentration was determined in terms of dry weight, iron content of the dry nanomaterial, and iron content in stock nanomaterial water suspensions as described.[38] The aqueous nanoparticle suspension was sterilized by ^{60}Co gamma-irradiation (dosage 25 kGy; Isotron Deutschland GmbH).[40] The mean magnetite crystallite size $\langle d \rangle$ was calculated from the broadening of the X-ray diffraction peaks using the Scherrer formula[41] (measurements kindly performed by Dr. Elena Oranskaya, The Ukranian Academy of Sciences). The mean hydrodynamic diameter, the polydispersity index (PI), and the zeta potential of the MNP suspension in water were determined by photon correlation spectroscopy (PCS) using a Malvern 3000 HS Zetasizer (U.K.). Magnetization and hysteresis loop measurements were kindly performed by Prof. Anna Slawska-Waniewska (Institute of Physics, Polish Academy of Sciences) at 298 K with a vibrating sample magnetometer (Oxford Instruments Ltd.) in the applied field ± 1.0 T. Electron spectroscopy for chemical analysis (ESCA) of the coating components and PEI-Mag2 nanomaterial were recorded and analyzed by Dr. Uwe Vohrer and Dr. Joachim Mayer (Fraunhofer Institute for Interfacial Engineering and Biotechnology) with a Kratos Analytical electron spectrometer (Manchester, U.K.) employing Al Kα excitation (1,486.6 eV). The samples were allowed to dry on a silicon wafer. An instrument vacuum of at least 10^{-9} mbar was maintained during analysis.

Adenoviruses. The E1A mutant adenovirus dl520 (Ad520), wild-type adenovirus (WT-Ad), and E1-minus adenovirus expressing luciferase (Ad-Luc) under the control of the cytomegalovirus promoter (CMV) were propagated in 293 cells and purified by double cesium chloride gradient centrifugation. Viral titers were determined to be 1×10^{10} infective units per mL (pfu/mL) and 1.34×10^{12} physical virus particles per mL (VP/mL) by an end-point dilution assay on 293 monolayers and UV optical absorbance (OD) at 260 nm with an extinction coefficient of 9.09×10^{-13}

(36) Holm, P. S.; Lage, H.; Bergmann, S.; Jurchott, K.; Glockzin, G.; Bernshausen, A.; Mantwill, K.; Ladhoff, A.; Wichert, A.; Mymryk, J. S.; Ritter, T.; Dietel, M.; Gansbacher, B.; Royer, H. D. Multidrug-resistant cancer cells facilitate E1-independent adenoviral replication: impact for cancer gene therapy. *Cancer Res.* **2004**, *64* (1), 322–8.

(37) Holm, P. S.; Scanlon, K. J.; Dietel, M. Reversion of multidrug resistance in the P-glycoprotein-positive human pancreatic cell line (EPP85−181RDB) by introduction of a hammerhead ribozyme. *Br. J. Cancer* **1994**, *70* (2), 239–43.

(38) Mykhaylyk, O.; Antequera, Y. S.; Vlaskou, D.; Plank, C. Generation of magnetic nonviral gene transfer agents and magnetofection in vitro. *Nat. Protoc.* **2007**, *2* (10), 2391–411.

(39) Mykhaylyk, O.; Vlaskou, D.; Tresilwised, N.; Pithayanukul, P.; Moller, W.; Plank, C. Magnetic nanoparticle formulations for DNA and siRNA delivery. *J. Magn. Magn. Mater.* **2007**, *311*, 275–81.

(40) Kowalski, J. B.; Tallentire, A. Substantiation of 25 kGy as a sterilization dose: a rational approach to establishing verification dose. *Radiat. Phys. Chem.* **1999**, *54* (1), 55–64.

(41) Kril, C. E.; Birringer, R. Estimating grain-size distributions in nanocrystalline materials from X-ray diffraction profile analysis. *Philos. Mag. A* **1998**, *77* (3), 621–40.

OD mL × cm/virion,[42] respectively. The preparation yielded 134 VP per pfu. Virus suspension aliquots were stored at −80 °C in PBS^{2+}/10% glycerol buffer (0.49 mM $MgCl_2$, 0.68 mM $CaCl_2$ and 10% glycerol in PBS) or 10 mM Tris buffer; pH 7.4 containing 2.5% glycerol.

Hydrated Particle Diameter, Electrokinetic (Zeta) Potential, Colloidal Stability, and Magnetic Responsiveness of Ad520−PEI-Mag2 Complexes. Hydrated particle diameters and electrokinetic or ξ-potentials were determined by PCS. For this purpose, 450 μL of Ad520 diluted in OptiMEM comprising 2.68×10^8 VP and 50 μL of a dilution series of PEI-Mag2 magnetic particles in water were mixed to obtain nanoparticle-to-viral-particle ratios of 2.5−40 fg of Fe/VP and allowed to associate for 20 min. For ξ-potential measurements, the resulting complexes were diluted in 1.5 mL of OptiMEM, PBS or cell culture medium. To investigate the effect of virus particle concentration (2×10^9 to 4×10^{10} VP/mL) and of the medium (PBS or OptiMEM) during complex assembly at a MNP-to-VP ratio of 5 fg of Fe/VP on the size, electrokinetic potential and magnetic responsiveness of the complexes, we prepared the complexes by mixing 48 μL of the virus stock (4.5×10^{10} VP/mL) with 0, 54, 108, 216, 432, 864 or 1,026 μL of PBS or OptiMEM followed by adding to and mixing with 6 μL of PEI-Mag2 stock (2.5 μg of Fe/μL). The mixture was allowed to associate for 20 min and adjusted to a total volume of 1,080 μL with PBS or OptiMEM, respectively. The resulting complexes were used for measurements of the size, ξ-potential and magnetic responsiveness. For complex formation at various MNP-to-VP ratios in the range of 0.625−40 fg of Fe/VP, the amounts of the PEI-Mag2 stock used for assembling the complexes were adjusted accordingly. For characterization of the complexes assembled at high virus concentration of 1.79×10^{11} VP/mL, the complexes were prepared as described below for in vivo application in a murine xenograft model.

The sedimentation stability and magnetic responsiveness of Ad520−PEI-Mag2 complexes were determined using a turbidity measurement both without magnetic field application and when subjected to inhomogeneous magnetic fields, respectively, as recently described.[43,44] Briefly, 500 μL aliquots of Ad520−PEI-Mag2 complexes, prepared as described for particle size and electrokinetic potential measurements, were placed in an optical cuvette placed in a spectrophotometer (Beckman DU 640) and exposed to a defined magnetic field gradient; the time course of optical density at 300 nm was then recorded. The gradient field was generated by positioning two mutually attracting packs of four quadrangular neodymium−iron−boron (Nd−Fe−B) permanent magnets (17 × 17 × 4 mm) symmetrically on each side of the cuvette holder and parallel to the light beam. The resulting magnetic field was measured in a 1 mm grid in planes at different distances from the surface of the Nd−Fe−B magnet packs using a Hall probe. The z-component of the field gradient perpendicular to the surface of the magnets was calculated. In the measuring window, the magnetic field was rather uniform in the $X-Y$ plane parallel to both the surface of the magnets and measuring light beam, with a magnetic induction $\langle B \rangle$ and a field gradient $\langle \nabla B \rangle$, both perpendicular to the light beam, of 213 mT and 4 T/m, respectively. To establish the correlation between the measured optical density and the virus concentration in suspensions of complexes in the cuvette, 20 μL aliquots of the suspensions prepared at 5 fg of Fe/VP and 20 fg of Fe/VP with ^{125}I-labeled virus were sampled at different time points in the course of magnetophoresis in parallel with the turbidity measurements. The virus concentration was quantified with a gamma counter (shown in Figure 3B).

Studies on Adenovirus Association and Magnetic Sedimentation with Magnetic Nanoparticles and Stability of the Complexes in the Presence of FCS. Radioiodination of the virus was performed as described in the Supporting Information. A virus stock of 1.2×10^{12} VP/mL was prepared by mixing 1 volume of radioactive-labeled virus (2.6×10^{10} VP/mL with a radioactivity of 2.6 kBq/μL) with 9 volumes of unlabeled virus (1.34×10^{12} VP/mL). Magnetic complexes were prepared in PBS or OptiMEM as described above. After 20 min incubation at RT for assembling the complex, 80 μL of the resulting complexes were transferred into the wells of a U-bottom 96-well plate, which already contained 80 μL of OptiMEM, PBS or FCS, and then incubated for 10 or 30 min. To sediment the magnetic complexes, the plate was placed on a 96-magnet plate (OZ Biosciences, Marseille, France) for 1 h. One hundred microliters of each supernatant were carefully collected for gamma counting using a Wallac 1480 Wizard 3 automatic gamma counter (Finland). The percentages of virus particles associated and magnetically sedimented with MNPs in OptiMEM, PBS or 50% FCS were calculated as follows:

$$\%\ \text{virus}_{\text{bound}} = \left[1 - \frac{\text{CPM}_{\text{sample}}}{\text{CPM}_{\text{ref}}}\right] \times 100$$

where CPM_{ref} is the measured radioactivity in terms of count per minute (CPM) in a probe from a reference (virus alone).

AFM. For TEM and AFM, adenovirus Ad520 was inactivated by a photochemical reaction with psoralen under exposure to long-wavelength UV light (320−380 nm).[45] Adenovirus associated with PEI-Mag2 magnetic particles was

(42) Mittereder, N.; March, K. L.; Trapnell, B. C. Evaluation of the concentration and bioactivity of adenovirus vectors for gene therapy. *J. Virol.* **1996**, *70* (11), 7498–509.

(43) Mykhaylyk, O.; Zelphati, O.; Hammerschmid, E.; Anton, M.; Rosenecker, J.; Plank, C. Recent advances in magnetofection and its potential to deliver siRNAs in vitro. *Methods Mol. Biol.* **2009**, *487*, 111–46.

(44) Mykhaylyk, O.; Zelphati, O.; Rosenecker, J.; Plank, C. siRNA delivery by magnetofection. *Curr. Opin. Mol. Ther.* **2008**, *10* (5), 493–505.

(45) Hanson, C. V.; Riggs, J. L.; Lennette, E. H. Photochemical inactivation of DNA and RNA viruses by psoralen derivatives. *J. Gen. Virol.* **1978**, *40* (2), 345–58.

prepared by mixing inactivated Ad520 (1.5×10^8 VP) and PEI-Mag2 nanoparticles (0.75 μg of Fe) in a total volume of 50 μL in OptiMEM resulting in a MNP-to-VP ratio of 5 fg of Fe/VP and a virus concentration of 3.0×10^9 VP/mL. After 20 min incubation, 2 μL aliquots of the complexes as well as both virus and magnetic particles alone were applied to smooth and clear mica surfaces and air-dried. Next, the samples were carefully rinsed with 50 μL of double-distilled water to remove buffer salts and then air-dried again. Imaging was performed in air using a NanoWizard I atomic force microscope (JPK Instruments AG, Berlin, Germany) coupled with an inverted Axiovert S100 microscope (Carl Zeiss AG, Oberkochen, Germany). Silicon cantilevers NSC36/AlBS with a force constant of 2 N/m and a resonance frequency of 150 kHz were used for imaging in tapping mode (or intermittent-contact mode). Images were acquired using the imaging software WSxM.[46]

TEM. Negative stain sample preparation was performed following the method of Stilwell et al.[47] with a slight modification. A Formvar/carbon-filmed 400 mesh copper grid was cleaned with hydrogen/oxygen gas for 30 s to remove hydrocarbon contamination on the grid using the Solarus advanced plasma cleaning system (Gatan GmbH). Virus (4.0×10^8 VP), PEI-Mag2 particles alone (0.25 μg of Fe), or magnetic virus complexes were prepared in a total volume of 12 μL in OptiMEM resulting in a MNP-to-VP ratio of 0.625 fg of Fe/VP and a virus concentration of 3.3×10^{10} VP/mL. A 5 μL drop of the complex sample was placed onto the grid and incubated for 10 min. Samples were rinsed cautiously with two drops of double-distilled water to remove buffer salts and then stained with 10 μL of 1% phosphotungstic acid aqueous solution (Electron Microscopy Sciences) for 3 min, except the grid with PEI-Mag2 particles alone. All samples were subsequently air-dried prior to imaging at an accelerating voltage of 80 kV using a TITAN 80-300 S/TEM (FEI Company).

Preparation of Adenovirus−Magnetic Nanoparticle Infection Complexes. The magnetic virus complexes were prepared by mixing either 40 μL of a dilution series of PEI-Mag2 magnetic nanoparticle suspension in water or 40 μL of water (as a reference) with 7.72×10^8 VP or 5.76×10^6 pfu diluted in 320 μL of OptiMEM. The concentration of magnetic nanoparticles was in the range of 6.03 to 772 μg of Fe/mL, resulting in nanoparticle-to-VP ratios from 0.3125 to 40 fg of Fe/VP. After 20 min incubation at RT, 2-to-1 dilutions of the complexes were performed to cover the multiplicities of infection (MOIs) from 80 to 0.625 (for virus−magnetic-nanoparticle complexes) when 50 μL of the complexes were added to cells seeded at a density of 10,000 cells per well in a 96-well plate. Adenovirus Ad520 and Ad-Luc were utilized to prepare the complexes for testing oncolytic activity and cytotoxicity of the complexes, respectively.

Infection Experiment in 96-Well Plate Format. 181RDB-fLuc and HeLa-P cells were seeded in flat-bottom 96-well plates at 10,000 cells per well. Twenty-four hours later, the medium in each well was replaced with 150 μL of fresh cell culture medium containing 10% FCS; 50 μL of Ad520, Ad-Luc (negative control) or WT-Ad (positive control) associated with MNPs or virus alone, prepared as described above, was added to the cells. The final concentration of FCS in the cell culture medium after addition of the infection medium was 7.5%. Cells were infected with viruses or magnetic virus complexes with or without positioning on the 96-magnet plate for 30 min after addition of the viruses and magnetic virus complexes. No medium change was performed, and the cells were further cultured for 6 days (unless otherwise stated). Uninfected cells were used as a reference. To compare the oncolytic effect between infection in 7.5% and 50% FCS, the medium was replaced 24 h post-cell seeding with 150 μL of fresh cell culture medium containing 10% FCS or 66.7% FCS, followed by addition of 50 μL of infection medium, resulting in final FCS concentrations of 7.5% or 50%, respectively. At 24 h postinfection, the medium was replaced with fresh cell culture medium, and the cells were further cultivated until evaluation. All samples were measured in triplicate. Cell survival was assessed by a luciferase assay in cells stably expressing luciferase or by a MTT-based respiration activity assay.[48,49]

MTT Assay. Infected cells and untreated reference cells were washed with PBS and incubated for 2−3 h with 100 μL of 1 mg/mL MTT solution prepared in PBS with 5 mg/mL glucose. Afterward, 100 μL of solubilization solution (10% Triton X-100 in 0.1 N HCl in anhydrous isopropanol) was added to dissolve the formazan. The optical density was measured at 590 nm. Cell viability was expressed as respiration activity normalized to the reference data for untreated cells.

Luciferase Assay. The cells were washed with PBS and lysed with 100 μL of lysis buffer (0.1% Triton X-100 in 250 mM Tris; pH 7.8) per well. After incubation for 15−20 min at RT, 50 μL of cell lysate in each well was transferred into a 96-well black flat-bottom plate, and then 100 μL of luciferase buffer was added. To evaluate the oncolytic activity at different time points, cells were seeded in 96-well black plates with flat and clear bottoms and infected as explained above. At the indicated time point, cells were washed with PBS, and 100 μL of 35 μM D-luciferin in PBS was added.

(46) Horcas, I.; Fernandez, R.; Gomez-Rodriguez, J. M.; Colchero, J.; Gomez-Herrero, J.; Baro, A. M. WSXM: a software for scanning probe microscopy and a tool for nanotechnology. *Rev. Sci. Instrum.* **2007**, *78* (1), 013705.

(47) Stilwell, J. L.; McCarty, D. M.; Negishi, A.; Superfine, R.; Samulski, R. J. Development and characterization of novel empty adenovirus capsids and their impact on cellular gene expression. *J. Virol.* **2003**, *77* (23), 12881–5.

(48) Berridge, M. V.; Herst, P. M.; Tan, A. S. Tetrazolium dyes as tools in cell biology: new insights into their cellular reduction. *Biotechnol. Annu. Rev.* **2005**, *11*, 127–52.

(49) Mueller, H.; Kassack, M. U.; Wiese, M. Comparison of the usefulness of the MTT, ATP, and calcein assays to predict the potency of cytotoxic agents in various human cancer cell lines. *J. Biomol. Screening* **2004**, *9* (6), 506–15.

Chemiluminescence intensity (count time of 0.20 min with background correction) was measured using a Microplate Scintillation & Luminescence Counter (Canberra Packard). After chemiluminescence measurements, the cells were washed with PBS, cell culture medium was added, and the cells were further cultivated. To construct a calibration curve, cells were seeded in the 96-well black plate with flat and clear bottoms at densities of 300−20,000 cells per well. After cell adhesion, chemiluminescence intensity was measured from living cells as described above. Untreated cells were used as a reference. Cell viability was expressed as the number of cells per well normalized to the reference data (%).

Evaluation of Virus Internalization into Cells. Cells were infected with a mixture of ^{125}I-labeled and unlabeled Ad520 (1:1) under the same infection conditions as described above for the infection experiment in 96-well plate. After 6 h infection, the cells were washed with PBS and treated with 100 units/mL heparin solution for 20 min at 37 °C. Next, the cells were washed with PBS and then lysed with 50 μL of lysis buffer. The cell lysate in each well was carefully collected using a pipet, transferred into a scintillation vial, and counted using the gamma counter. All of the experiments were done in triplicate. The applied virus doses were counted as reference data. Internalized virus particles per cell were calculated as follows:

$$\text{internalized VP/cell} = \frac{\text{CPM}_{\text{sample}}}{\text{CPM}_{\text{applied}}} \times \text{applied VP/cell}$$

where $\text{CPM}_{\text{applied}}$ is the measured radioactivity of the applied virus dose.

Dose−Response Curve Analysis. Cell survival as a percentage of the reference (untreated cells) was plotted against the logarithm of the applied virus dose [LOG (MOI)]. The modified Hill model[50,51] was used to describe experimental dose−response curves and the effect of exposure time on the concentration of virus required to generate a specific outcome. Fitting to the logistic function with the variable Hill slope factor "*p*" was performed using OriginPro8 Data Analysis Software (http://www.originlab.com). Cell survival was calculated as follows:

$$\text{living cells (\%)} = A_1 + \frac{A_2 - A_1}{1 + 10^{[\log(\text{IC}_{50}) - \log(\text{MOI})]p}}$$

where A_1 is cell survival at infinite virus concentration (the lower asymptote), A_2 is the upper asymptote, and IC_{50} is the concentration of virus resulting in 50% of the maximal effects (cell growth inhibition).

Infection Experiment in Six-Well Plate Format. To examine progeny viral particle production and viral DNA replication and to demonstrate a magnetically targeted oncolytic effect, 1.5×10^5 181RDB cells in 2 mL of cell culture medium per well were seeded in a 6-well plate and incubated for 48 h prior to infection. The medium was replaced with 1,920 μL of OptiMEM and 80 μL of adenoviruses alone or their complexes (Ad−PEI-Mag2). Complexes were prepared to comprise a nanoparticle-to-virus particle ratio of 5 fg of Fe/VP and a desired MOI of 10 with respect to the originally seeded cells. Cells were infected without or with incubation on the 96-magnet plate for 15 min after adding the viruses and magnetic virus complexes. Except when the magnetically targeted and confined oncolysis was tested, Nd−Fe−B disk magnets (15 × 15 mm) were placed below the centers of individual wells. Subsequently, the infection medium was substituted with 2 mL of fresh cell culture medium, and the cells were further incubated until assessment. For investigating viral progeny production and viral DNA replication, Ad-Luc and WT-Ad were used as a negative and a positive control, respectively.

Sulforhodamine B Staining of Cellular Protein. Cell growth inhibition six days postinfection in a six-well plate format was visualized with sulforhodamine B (SRB) staining.[52] The cells were washed with PBS and fixed with 10% trichloroacetic acid for 1 h at 4 °C. Next, the fixed cells were washed with water, stained with 0.5% SRB in 1% acetic acid solution for 15 min, washed with 1% acetic acid to remove excess dye, and allowed to air-dry at RT.

End-Point Dilution Assay. Five days postinfection, viruses were harvested from the infected cells by 3 cycles of freezing−thawing followed by centrifugation at 3,000 rpm for 15 min. The supernatants were tested for virus production by end-point dilution assays on 293 cells according to the manufacturer's instruction (BD Biosciences Clontech). Viral titers were calculated in terms of pfu/mL.

Southern Blot Analysis. To assess viral DNA replication 3 days postinfection, the infected cells were harvested and digested in digestion buffer (0.5% SDS, 100 mM NaCl, 10 mM Tris-Cl (pH 8.0), 25 mM EDTA (pH 8.0) in water) containing 1% QIAGEN proteinase K by shaking at 600 rpm, 50 °C overnight. Genomic DNA was isolated by phenol−chloroform extraction. Four micrograms of isolated DNA was digested with restriction endonuclease *Kpn*I, size fractionated on a 1% agarose gel, and transferred to a nylon membrane using the Turboblotter Rapid Downward Transfer Systems (Schleicher&Schuell, Germany). The membrane was hybridized with a ^{32}P-labeled adenovirus E2A-cDNA probe to detect adenoviral DNA replication.[36] The blot was visualized using a Phosphor-Imager (Fuji FLA 2000). DNA isolated from uninfected cells was used as a negative control.

Growth of Tumor Xenografts in Nude Mice Following Local Injection of Ad520−PEI-Mag2 Magnetic Complexes. Xenografts were established in 4-week-old female BALB/c nude *(nu/nu)* mice (Charles River, Sulzfeld, Germany) with an average body weight of 16.8 ±

(50) Barcroft, J.; Hill, A. V. The nature of oxyhaemoglobin, with a note on its molecular weight. *J. Physiol.* **1910**, *39* (6), 411–28.
(51) Levasseur, L. M.; Slocum, H. K.; Rustum, Y. M.; Greco, W. R. Modeling of the time-dependency of in vitro drug cytotoxicity and resistance. *Cancer Res.* **1998**, *58* (24), 5749–61.
(52) Skehan, P.; Storeng, R.; Scudiero, D.; Monks, A.; McMahon, J.; Vistica, D.; Warren, J. T.; Bokesch, H.; Kenney, S.; Boyd, M. R. New colorimetric cytotoxicity assay for anticancer-drug screening. *J. Natl. Cancer Inst.* **1990**, *82* (13), 1107–12.

1.1 g by injecting 1.5×10^6 daunorubicin-resistant human pancreatic carcinoma cells stably expressing firefly luciferase (181RDB-fLuc cells) suspended in 200 μL of 25% Matrigel (BD Biosciences, San Jose, CA) in sterile 5% glucose subcutaneously into the right flank. The tumor size was measured twice weekly in two dimensions by a digital caliper. Tumor volumes were estimated by the formula: $4/3\pi \times \text{length}/2 \times (\text{width}/2)^2$. When the tumors reached volumes between 150 to 300 mm^3 after 2 weeks of growth, the mice were randomized into three groups of five animals each. The animals received three injections each of oncolytic adenovirus Ad520 (Ad520 group), its magnetic complexes (Ad520−PEI-Mag2 group) in 75 μL of PBS or just 75 μL of PBS (reference group) intratumorally on days 0, 7, and 11 of treatment. The average tumor volumes at the day of the first treatment (day 0) were 277 ± 106 mm^3 in the Ad520 group, 225 ± 72 mm^3 in the Ad520−PEI-Mag2 group and 243 ± 134 mm^3 in the PBS group.

For preparing Ad520−PEI-Mag2 complexes for in vivo injection, 10 μL of virus stock (1.34×10^{10} VP or 1×10^8 pfu) was diluted with 38.2 μL of PBS and mixed with 26.8 μL of PEI-Mag2 nanoparticle suspension containing 67 μg of Fe. This resulted in a MNP-to-VP ratio of 5 fg of Fe/VP and a virus concentration of 1.79×10^{11} VP/mL. The complexes were injected after 20 min incubation at room temperature. Immediately after injection, the anesthetized mice were positioned such that the tumors touched the surface of a cylindrical Nd−Fe−B magnet. The magnet consisted of two stacked disk-shaped NeoDelta magnets (NE155; $d = 15$ mm, $h = 5$ mm; IBS Magnet, Berlin, Germany). The mice were left under magnetic field influence for 30 min. For the nonmagnetic treatment, the same amount of virus was diluted to 75 μL with PBS and injected without magnetic field application. The control group received 75 μL of PBS without magnetic field application.

For in vivo luminescence imaging, the mice were anesthetized and administered 200 μL of D-luciferin (SYNCHEM OHG, Germany) in sterile PBS at a dose of 150 mg/kg intraperitoneally. Ten minutes later, photons from the right flank were counted using the IVIS 100 Imaging System (Xenogen, USA). The data were analyzed by using Living Image 2.50 software (Xenogen, USA). To compensate for mouse-to-mouse variability, the data on tumor volume and integral luminescence intensity were normalized to the values measured for each mouse at day 0 of treatment.

Adenovirus DNA Replication Post Intratumoral Injection in Mice. For regular PCR analysis after digestion of tumor and liver tissues, the genomic DNA was extracted by phenol−chloroform and precipitated with ethanol. One microgram of the purified DNA, 5 units of Taq DNA polymerase (Fermentas), 0.25 μmol/L forward and reverse primers, and PCR buffer were mixed in a final volume of 50 μL. To amplify the hexon gene, the forward primer 5′-GGCCATTACCTTTGACTCTTC-3′ and reverse primer 5′-GCATTTGTACCAGGAACCAGTC-3′ were used. The purified DNA from adenovirus Ad520 and the purified DNA isolated from tumor or liver of a mouse in a reference PBS group were used as a positive and a negative control, respectively. One cycle consisting of 30 s denaturation at 95 °C, 30 s annealing at 53 °C and 30 s extension at 72 °C using a RoboCycler Gradient 40 (Stratagene, The Netherlands) was carried out for 30 cycles. The PCR products were electrophoresed on 1% agarose gels and visualized by staining with ethidium bromide.

Non-Heme Iron Determination. To determine non-heme iron content in tumor, liver, lungs, spleen, kidneys and heart tissues, 100 μL samples after digestion of the tissue were incubated overnight at 65 °C with 250 μL of acid mixture containing 3 M hydrochloric acid and 0.61 M trichloroacetic acid. Clear supernatant was used for non-heme iron determination by a colorimetric method with 1,10-phenanthroline as described.[38] Briefly, 50 μL of the supernatant was mixed with 70 μL of double distilled water, 20 μL of 10% hydroxylamine hydrochloride solution, 100 μL of ammonium acetate buffer and 50 μL of 0.1% 1,10-phenanthroline solution. The mixture was incubated for 20 min at RT, and the optical density at 510 nm was measured against blank.

Statistical Analysis. Data are presented as mean ± SD. Comparisons between two means were made by t tests. Analysis of variance was performed by ANOVA procedures using SPSS Statistics 17.0 (SPSS, Inc.). Significance of the differences between means was tested using post hoc Tukey's and Dunnett's T3 pairwise comparison tests when the variances were equal and unequal, respectively. A $p < 0.05$ was taken as the cutoff for significance.

Results

PEI-Mag2 Magnetic Nanoparticles. The PEI-Mag2 magnetic nanoparticles used for association with adenovirus particles were obtained by aqueous synthesis as previously described.[38] A brief overview of the particle characteristics is given in Table 1. PEI-Mag2 particles with magnetite cores have a mean crystallite size, $\langle d \rangle$, of 9 nm according to X-ray diffraction analysis (Figure S1 in the Supporting Information). The average core diameter, $\langle d_{TEM} \rangle$, evaluated from the transmission electron microscopy (TEM) data (shown in Figure 4, top panel) was 10.2 ± 2.2 nm. The hydrodynamic diameter in aqueous suspension was 28 ± 2 nm and was in good agreement with the mean particle size, D_{AFM}, determined from AFM images (32 ± 10 nm, $n = 62$; shown in Figure 4, bottom panel).

Figure 1A (III) shows a schematic representation of the core−shell magnetite nanoparticles that demonstrate superparamagnetic behavior (no remanent magnetization) at room temperature (RT) (magnetization curve given in Figure 1B). The particles were stabilized with 25 kDa branched polyethylenimine (PEI-25_{Br}) combined with the fluorinated surfactant ZONYL FSA. Structural formulas of the materials are provided in Figure 1A (I and II). Fluorinated surfactants form stable, mixed, self-assembling layers with surfactants and polymers.[53] The anchoring of the surfactant (component

(53) Riess, J. G. Fluorous micro- and nanophases with a biomedical perspective. *Tetrahedron* **2002**, *58* (20), 4113–4131.

Table 1. Characteristics of the Core−Shell Type PEI-Mag2 Magnetic Nanoparticles

characteristics	results
phase composition of the core	magnetite
mean crystallite size of the core, $\langle d \rangle$ (nm)	9
mean core diameter, $\langle d_{TEM} \rangle$ (nm)[a]	10.2 ± 2.2
saturation magnetization of the core, M_s (A m^2/kg of Fe)	62
av iron wt per particle, P^{Fe}_{part} (g of Fe/particle)[b]	1.4×10^{-18}
effective magnetic moment of the particle, m_{eff}(A m^2)[c]	8.7×10^{-20}
iron content (g of Fe/g dry wt)	0.56
stabilizer content (g/g dry wt)	0.23
mean hydrated particle diameter in water, D_h (nm)	28 ± 2
polydispersity index, PI	0.20 ± 0.02
mean particle size, D_{AFM} (nm)[d]	32 ± 10
shell composition[e]	PEI-25$_{Br}$ (32 mass%) and ZONYL FSA (68 mass%)
electrokinetic potential in water, ξ (mV)	+55.0 ± 0.7

[a] Derived from transmission electron microscopy (TEM) data. [b] Calculations account for magnetite structure and crystallite size of the core of the particles. [c] Calculated based on the core crystallite size and magnetization in a magnetic field of 213 mT. [d] Derived from atomic force microscopy (AFM) data. [e] Based on ESCA data shown in Figure 1.

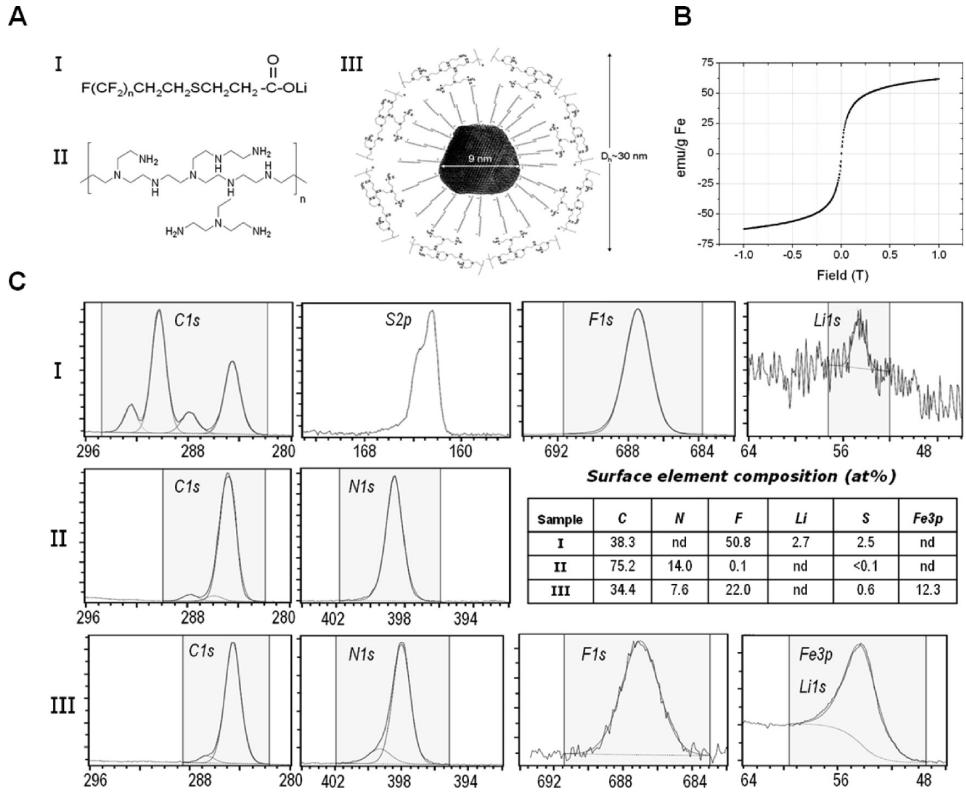

Figure 1. Characteristics of core−shell type PEI-Mag2 magnetic nanoparticles. (A) Structural formulas of the coating components of the particles: (I) fluorinated surfactant lithium 3-[2-(perfluoroalkyl)ethylthio]propionate; (II) 25 kDa branched polyethylenimine; and (III) schematic of the nanoparticles comprising the magnetite core and a shell of self-assembled coating components I and II. (B) Magnetization curve of the nanoparticles at 298 K. (C) Selected fragments of ESCA spectra and relative elemental composition of the coating components (I and II) and the nanoparticles (III) (for nanoparticles based on Fe 3p peak); nd = nondetectable.

I) at the surface of iron oxide nanocrystals can occur due to coordination of the carboxylic groups with surface iron atoms of the magnetite core. PEI (component II) can bind nucleic acids by electrostatic interactions and is an excellent transfection reagent.[54] PEI can be assembled at the surface by electrostatic interaction with anionic carboxyl groups of the surfactant and by hydrophobic interactions. Electron spectroscopy for chemical analysis (ESCA) (Figure 1C) suggests that both coating components assemble at the surface of the particles, which allows evaluation of the composition of the

(54) Boussif, O.; Lezoualc'h, F.; Zanta, M. A.; Mergny, M. D.; Scherman, D.; Demeneix, B.; Behr, J. P. A versatile vector for gene and oligonucleotide transfer into cells in culture and in vivo: polyethylenimine. *Proc. Natl. Acad. Sci. U.S.A.* **1995**, *92* (16), 7297–301.

Table 2. Physicochemical Characteristics of the Complexes of Adenovirus Ad520 with PEI-Mag2 Magnetic Nanoparticles

nanoparticle-to-virus ratio at complex preparation				zeta potential, ξ (mV)				
fg of Fe/VP	MNP/VP	mean hydrodynamic diameter, D_h (nm)[a]	polydispersity index, PI[a]	in OptiMEM or PBS[a]	in cell culture medium[a,b]	av velocity, v_z (μm/s)[c,d]	magnetic moment, M (10^{-16} A m^2)[c]	no. of MNPs associated with complex
Complexes Assembled in OptiMEM at Virus Concentration of 5.4×10^8 VP/mL								
0	0	159 ± 12	0.46	−18.0 ± 3.7	−5.6 ± 2.8			
2.5	1,736	438 ± 219	0.50	+5.0 ± 0.4	−9.8 ± 1.6	1.41	12.9	14,961
5	3,472	228 ± 65	0.25	+15.1 ± 1.7	−9.2 ± 0.7	0.87	4.1	4,778
10	6,944	206 ± 36	0.18	+18.9 ± 1.2	−8.3 ± 1.1	0.86	3.7	4,283
20	13,889	192 ± 9	0.11	+21.5 ± 1.7	−6.3 ± 1.1	0.95	3.8	4,407
40	27,778	298 ± 141	0.26	+21.9 ± 3.2	+0.3 ± 3.7	1.02	6.4	7,371
Complexes Assembled in PBS at Virus Concentration of 2.1×10^9 VP/mL								
0	0	200 ± 50	0.49	−9.1 ± 1.3	−6.0 ± 1.2			
0.625	434	354 ± 44	0.27	−3.8 ± 0.6	−8.8 ± 0.8	0.22	5.5	6,404
1.25	868	666 ± 83	0.26	+3.2 ± 0.8	−9.2 ± 0.4	0.35	4.9	5,689
2.5	1,736	186 ± 23	0.25	+16.1 ± 1.0	−7.3 ± 0.2	0.39	2.5	2,847
5	3,472	220 ± 55	0.24	+17.1 ± 0.9	−8.0 ± 0.6	0.55	3.1	3,612
10	6,944	246 ± 29	0.23	+14.7 ± 0.8	−7.1 ± 0.3	0.85	3.9	4,484
20	13,889	249 ± 76	0.25	+17.4 ± 1.1	−6.5 ± 0.4	0.95	5.9	6,844
40	27,778	319 ± 56	0.27	+16.9 ± 0.6	−5.3 ± 0.1	1.39	3.7	4,297

[a] Mean ± SD (n = 50). [b] Measured after 4-fold dilution of the complex with full cell culture medium containing 10% FCS. [c] Measured at $\langle B \rangle$ = 213 mT. [d] Measured at $\langle \nabla B \rangle$ = 4 T/m.

stabilizing layer. The C:S element ratio was 15.3, and C:Li was 14.2. From these ratios we estimated that n equals 10 in the structural formula of the fluorinated surfactant $F(CF_2)_nCH_2CH_2SCH_2CH_2C(O)OLi$ (i.e., $F_{21}C_{15}H_8O_2SLi$, MW = 657.9). The calculated F:C ratio of 1.4 is in good agreement with the experimentally determined ratio of 1.33 with accounting for possible orientation effects of the surfactant molecules. Data on surface elemental composition of the particles (F:N ratio of 22 to 7.6), accounting for the 42 Da PEI monomer unit, show that the shell contains 68 mass % fluorinated surfactant and 32 mass % PEI. Taking into consideration the known average weight of the particle and the stabilizer content (given in Table 1), these data result in an average of 366 FSA molecules assembled with an average of 5 PEI-25_{Br} molecules per nanoparticle. The presence of PEI in the surface layer results in a highly positive net ξ-potential of the particles when measured in water suspension (+55.0 ± 0.7 mV) and good stabilization of the particles against aggregation.

Self-Assembly of Adenovirus and PEI-Mag2 Magnetic Nanoparticles and Stability of Complexes in 50% Fetal Calf Serum (FCS). Adenovirus particles have a negative zeta potential both in OptiMEM (−18.0 ± 3.7 mV) and in PBS (−9.1 ± 1.3 mV) (Table 2), while PEI-Mag2 particles have a strongly positive zeta potential (ξ = +55.0 ± 0.7 mV, Table 1). Hence, self-assembly of the virus with MNP is probably governed by electrostatic interaction. The extent of virus association and magnetic sedimentation with PEI-Mag2 and the complex stability in the absence and presence of 50% FCS were evaluated by determining supernatant radioactivity after magnetic sedimentation of complexes with radioactive-labeled virus. Figure 2A shows the percentage of magnetically sedimented viruses as a function of the magnetic particle-to-virus ratio in terms of iron weight per virus particle (fg of Fe/VP) for complexes assembled in serum-free OptiMEM at a virus particle concentration of 2×10^9 VP/mL. Maximum binding and sedimentation of up to 87% of viruses occur in OptiMEM in the range of 2.5−10 fg of Fe/VP. The stability of the complexes is reduced in 50% FCS. However, about 60% of virus was still magnetically sedimented in the range of 1.25−40 fg of Fe/VP after 30 min incubation in the presence of 50% FCS. More detailed data on the stability of the complexes assembled at virus concentrations between 2×10^9 and 2×10^{11} VP/mL are given in Figure S2 in the Supporting Information and are summarized in Figure 2D for complexes formulated at 5 fg of Fe/VP. The results provide evidence of high association of the virus with magnetic nanoparticles and high stability in the presence of 50% FCS for both the complexes assembled in OptiMEM and in PBS. The magnetophoretic mobility of the complexes was similar when measured in OptiMEM and 50% FCS (Figure S3 in the Supporting Information). Hence, the lower magnetic sedimentation of the virus in the presence of 50% FCS is predominantly due to partial dissociation of the virus−magnetic particle complexes.

Physical Characteristics of Ad520 Complexes with PEI-Mag2 Magnetic Nanoparticles. The data on zeta potentials of the complexes assembled in OptiMEM or PBS shown in Table 2 and plotted against nanoparticle-to-virus ratios in Figure 2B are consistent with the association of the negatively charged virus particles with positively charged PEI-Mag2 nanoparticles. This complex formation results in a corresponding shift of the zeta potential from negative to positive to a plateau about +20.0 mV at a magnetic particle-to-virus ratio above 10 fg of Fe/VP. As shown in Figure

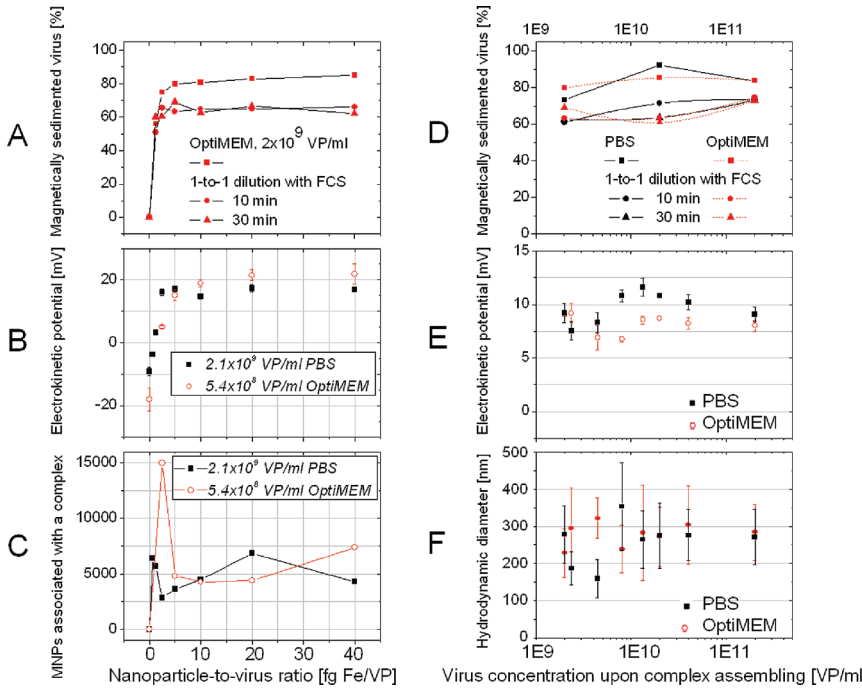

Figure 2. (A) Virus association with PEI-Mag2 magnetic nanoparticles, stability of the resulting complexes in 50% FCS, and magnetic sedimentation of the complexes. I^{125}-labeled virus and magnetic nanoparticles were mixed in OptiMEM at various nanoparticle-to-virus particle ratios at a final virus concentration after complex assembly of 2×10^9 VP/mL and were incubated for 20 min to form the complexes. The resulting complexes were 1-to-1 diluted with OptiMEM or FCS and then incubated for 10 or 30 min before positioning on the 96-magnet plate for 1 h to magnetically sediment the complexes. I^{125} radioactivity in the supernatants was measured to quantify the percentage of virus that associated and magnetically sedimented with MNPs. (B) The electrokinetic (zeta) potential and (C) number of MNPs associated with a complex versus nanoparticle-to-virus particle ratios when assembling the complex in PBS or in OptiMEM at a final virus concentration of 2.1×10^9 or 5.4×10^8 VP/mL, respectively. (D) Magnetic sedimentation and stability in 50% FCS, (E) the electrokinetic potential and (F) mean hydrodynamic diameter of the PEI-Mag2-Ad520 complexes assembled at nanoparticle-to-virus particle ratio of 5 fg of Fe/VP in PBS or OptiMEM versus virus concentrations upon assembling the complex.

2E, there is no significant difference between the zeta potentials of complexes prepared in OptiMEM or in PBS over the whole concentration range of 2×10^9 to 2×10^{11} VP/mL during assembly.

The Ad520−PEI-Mag2 complexes were around 200 nm in diameter at ratios of 5 to 20 fg of Fe/VP. There were no significant differences in physicochemical characteristics when the complexes were assembled in OptiMEM or PBS (Table 2) or at different virus concentrations (Figure 2F). At low magnetic particle-to-virus ratios, the zeta potential is close to neutral (-3.8 ± 0.6 mV or $+5.0 \pm 0.4$ mV for complexes formulated at 0.625 fg of Fe/VP in PBS or at 2.5 fg of Fe/VP in OptiMEM, respectively) and the complexes aggregate. Complexes with the high ratio of 40 fg of Fe/VP also display large diameters, presumably due to aggregation of unbound MNPs. In cell culture medium containing 7.5% serum, the apparent zeta potentials of virus alone and virus complexes turn toward neutral or slightly negative values, suggesting that opsonization of both virus alone and virus complexes takes place (Table 2).

Turbidity measurements of the Ad520 magnetic complex suspensions showed that except at low MNP/VP ratios (0.625−2.5 fg of Fe/VP) the complexes were colloidally stable during 2 h post-complex preparation in the absence of a magnetic field (data shown in Figure 3C). The clearance velocity under the influence of magnetic field gradient (shown in Figures 3B and 3D) is related to the magnetophoretic mobilities of the complexes, which in turn are proportional to their magnetic moments. Briefly, magnetic force that acts on a magnetic virus complex comprising multiple magnetic particles in the presence of the magnetic field gradient $\nabla\vec{B}$ is given by $\vec{F}_m = (\vec{M}\cdot\vec{\nabla})\vec{B}$. The total magnetic moment of the magnetic vector, $\vec{M}$, is the product of the effective magnetic moment, m_{eff}, of the MNP under the magnetic field, $\vec{B}$, and the total number, N, of magnetic particles associated with the complex ($\vec{M} = N\cdot\vec{m}_{eff}$). Above the saturation magnetization of the MNP, which is achieved with fields exceeding 200 mT for magnetite (Figure 1B), the magnetic force experienced by the magnetic dipole is a linear function of the field gradient. Magnetic complexes must move in the direction of the maximum magnetic field and are subjected to a hydrodynamic drag force that can be described by Stokes law as $\vec{F}_d = -3\pi\eta D_h\vec{v}$, where η is the viscosity of the carrier liquid, D_h is an average hydrodynamic diameter of the complex, and $\vec{v}$ is the velocity of the

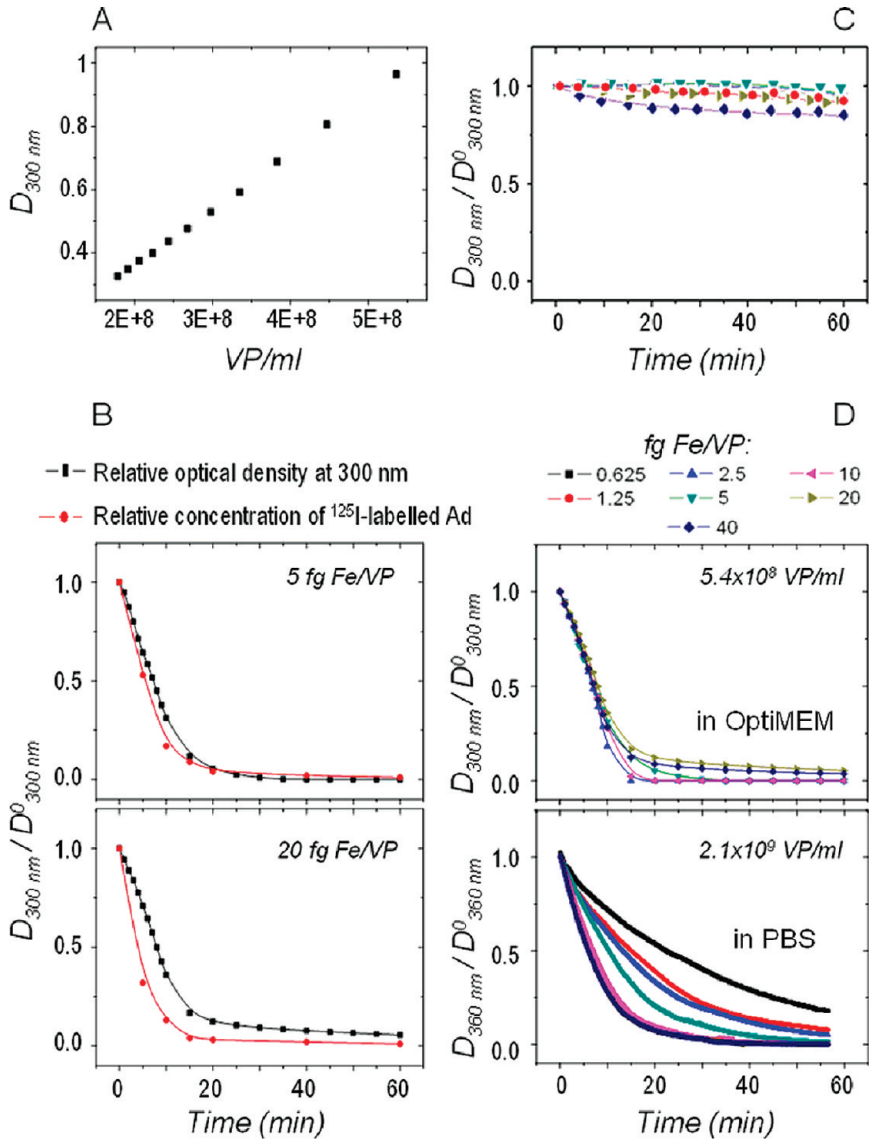

Figure 3. Sedimentation stability and magnetic responsiveness of the Ad520−PEI-Mag2 complexes. (A) Optical density at 300 nm registered for a dilution series of the complexes prepared at 20 fg of Fe/VP as a function of virus particle concentration in suspension, with no magnetic field applied. (B) Relative optical density and relative concentration of the I^{125}-labeled virus in suspensions of the complexes prepared at nanoparticle-to-virus ratios of 5 and 20 fg of Fe/VP versus time upon application of the inhomogeneous permanent magnetic field. Time course of the normalized turbidity of the magnetic virus complexes at various nanoparticle-to-virus particle ratios (fg of Fe/VP) (relative optical density normalized to the initial optical density, D/D^0) (C) without magnetic field application for complexes assembled at virus concentration of 5.4×10^8 VP/mL (the complexes were stable over 2 h. Only the first 60 min of the measurement are shown) and (D) upon application of an inhomogeneous permanent magnetic field for complexes assembled at virus concentrations of 5.4×10^8 VP/mL and 2.1×10^9 VP/mL in OptiMEM and PBS, respectively; plots assignment as shown in Figure 3D. The average magnetic field $\langle B_z \rangle$ value in the direction of complexes' movement perpendicular to the measuring light beam was 0.213 ± 0.017 T, and the magnetic field gradient in the direction of the complexes' movement was 4 ± 2 T/m.

complex. In a stationary regime, hydrodynamic drag force counterbalances the magnetic force. The average magnetic moment, M, of the complexes can then be calculated from the magnetically induced velocity in a magnetic field gradient as described by Wilhelm et al.[55] At a magnetic field $\langle B \rangle$ of 213 mT, which we have used in our experimental setup, the magnetization of the PEI-Mag2 nanoparticles according to the experimentally measured magnetization curve corresponds to 97% of the saturation value. Thus, the effective magnetic moment of each particle is $m_{\text{eff}} = (0.97 M_s) P^{\text{Fe}}_{\text{part}}$, where M_s is the specific saturation magnetization per unit iron weight and $P^{\text{Fe}}_{\text{part}}$ is the content of iron in one particle

(55) Wilhelm, C.; Gazeau, F.; Bacri, J. C. Magnetophoresis and ferromagnetic resonance of magnetically labeled cells. *Eur. Biophys. J.* **2002**, *31* (2), 118–25.

with a magnetite core equal in size to the average crystallite. Thus, the number of magnetite crystallites associated with a complex can be calculated from the magnetophoretic mobility, $\vec{v}$, estimated from the clearance curves as $N = 3\pi\eta D_h v/(\nabla B \cdot m_{eff})$. An average velocity, v_z, of the complexes under a magnetic field gradient was evaluated from the magnetic responsiveness curves as $v_z = \langle L \rangle / t_{0.1}$. Here $\langle L \rangle = 1$ mm is the average path of the complexes' movement perpendicular to the measuring light beam symmetrically in both directions to the surface of the magnets arranged from both sides of the 4 mm wide optical cuvette and $t_{0.1}$ is the time required for a 10-fold decrease in optical density. For all complexes assembled in PBS and OptiMEM at low nanoparticle-to-virus ratios of 2.5 to 10 fg of Fe/VP, the experimental clearance curves were well fitted to a single exponential decay curve, $y = A_1 \exp(-x/t_1)$, using OriginPro8 Data Analysis Software, and $t_{0.1}$ was calculated as $t_{0.1} = t_1 Ln(10)$. At high particle-to-virus ratios of 20 and 40 fg of Fe/VP, biphasic curves representing fast and slow component movements were observed (see Figures 3B and 3D). To assign the components, the time courses of both the optical density and the virus concentration were measured upon magnetic field application for complexes prepared at ratios of 5 and 20 fg of Fe/VP. Figure 3B clearly shows that the relative optical density curve almost coincides with the relative virus concentration curve for the complexes prepared at 5 fg of Fe/VP, whereas there is also a slow component observed when the complex was formulated at 20 fg of Fe/VP; this slow component apparently belongs to unbound magnetic particles and/or their aggregates. This observation is in agreement with photon correlation spectroscopy (PCS) results showing that, at magnetic particle-to-virus ratios equal to or higher than 10 fg of Fe/VP, the minor component is present in a size distribution curve that accounts for 5−20% of the scattered light intensity and belongs to the species with a hydrodynamic diameter of ca. 60 nm. Taking this datum into account, we assigned the fast major components of the clearance curves at high iron-to-virus ratios of 20 and 40 fg of Fe/VP to be the Ad520 complexes and the minor components to be the unbound magnetic particles/aggregates. Table 2 shows the average velocity, the magnetic moment of the complexes derived from these data, and the estimated number of MNPs associated with a complex (see also Figure 2C). Complexes prepared in OptiMEM at 5−10 fg of Fe/VP at low VP concentration (5.4×10^8 VP/mL) comprise 3,600 to 4,500 MNPs. Similar results were obtained with complexes prepared in PBS at an about 4-fold higher concentration (2.1×10^9 VP/mL). The mean hydrodynamic diameters of the complexes were ca. 200 nm, suggesting that the complex consists of one virus particle surrounded with the determined number of MNPs. Because aggregation occurs at lower MNP-to-virus ratios as well as with excess amounts of magnetic particles, the useful MNP-to-virus ratios for infection experiments are between 5 and 10 fg of Fe/VP.

Apart from providing information about the composition of complexes, the turbidity time course upon magnetic field application allows for the estimation of the necessary incubation time at the magnetic plate for sedimenting the complexes at the cell surface for in vitro infection experiments. Experimental curves in Figures 3B and 3D show that the suspension of complexes formulated at useful MNP-to-virus ratios between 5 and 10 fg of Fe/VP are completely cleared in less than an hour when subjected to a magnetic field $\langle B \rangle$ of 0.213 T and magnetic field gradient of 4 ± 2 T/m in the direction of the complexes' movement. A 96-magnet plate creates in a single well an average field of approximately 0.107 T and an average field gradient perpendicular to the well bottom of 55 T/m. Hence, 15 to 30 min of incubation at the magnetic plate is enough for complete magnetic sedimentation of the magnetic virus complexes.

Morphology of Ad520−PEI-Mag2 Complexes. AFM and TEM were performed to visualize magnetic virus complexes (Figure 4). According to TEM data, the electron-dense magnetite core of the PEI-Mag2 particles has an average diameter of 10.2 ± 2.2 nm, which is in good agreement with the crystallite size of 9 nm determined from X-ray line broadening using Scherrer's formula. The particle size of 32 ± 10 nm ($n = 62$) calculated from AFM images was comparable with the mean hydrodynamic diameter of 28 ± 2 nm from PCS analysis. Comparison with the hydrodynamic diameter of the magnetic particles (Table 1) suggests that the surface coating occupies a layer that is 9.5 nm thick. AFM images of the oncolytic adenovirus showed a particle diameter of 101 ± 20 nm ($n = 80$) ranging from 62 to 142 nm, consistent with the TEM data (105 ± 9 nm, $n = 7$). AFM of Ad520 magnetic complexes showed irregular objects of 171 ± 17 nm in diameter, putatively displaying virus particles decorated with multiple magnetic particles. These objects were frequently found in clusters, potentially as a result of the drying step during sample preparation but also possibly reflecting the actual situation in aqueous suspension, i.e., a magnetic particle surface layer that bridges several virus particles. TEM data support this interpretation, with both single virus particles that are surrounded by an electron-dense layer of MNPs and also clusters of several virus particles that are "embedded" in a magnetic particle background. The electron diffraction pattern taken from a sample of magnetic virus complexes originated from magnetite cores of PEI-Mag2 nanoparticles associated with the virus. Moreover, the intact icosahedral structure of adenovirus particles was clearly evident in the magnetic complexes.

The Ad520-Mediated Oncolytic Effect Is Enhanced by Magnetically Enforced Infection in CAR-Deficient Multidrug-Resistant 181RDB-fLuc Cells. To investigate the effect of serum protein concentrations on the oncolytic effect of adenovirus Ad520 alone and its magnetic complexes, infection in the presence of 7.5% and 50% FCS was performed. Figure 5A shows 181RDB-fLuc cell survival normalized to survival of the untreated cells as a reference plotted against the logarithm of the applied virus dose at 6 days postinfection. At high virus doses of 160 and 320 multiplicities of infection (MOIs) or plaque-forming units per cell (pfu/cell), the oncolytic effect of Ad520 in a medium

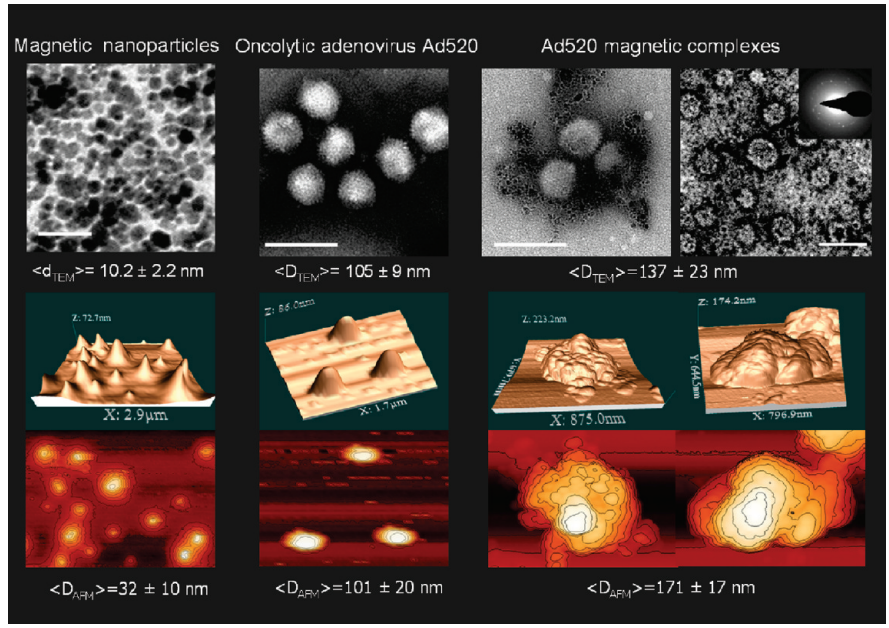

Figure 4. Morphology of oncolytic adenovirus magnetic complexes. Transmission electron microscopy (TEM) data (top panel) and atomic force microscopy (AFM) 3D images and contour plots (bottom panel) of the PEI-Mag2 magnetic nanoparticles, oncolytic adenovirus Ad520, and Ad520 magnetic complexes prepared at 5 fg of Fe/VP (unless otherwise indicated). The inset in the upper right TEM image of magnetic virus complexes shows an electron diffraction pattern from MNPs associated with the virus. Scale bars are 50 nm for the TEM image of the particles and 200 nm for the TEM images of the virus and its magnetic complexes. Average diameter $\langle D \rangle$ of the MNPs, virus particles, and their magnetic complexes (mean ± SD) evaluated from TEM and AFM data are shown in the figure.

containing 50% FCS was significantly ($p < 0.001$) lower than that in a medium containing 7.5% FCS. However, there was no statistically significant difference between the oncolytic effects of Ad520−PEI-Mag2 complexes in 7.5% and 50% FCS. When a magnetic field was applied to enforce target cell contact of the complexes, oncolytic activity was enhanced approximately 10-fold by decreasing the IC_{50} (Table 3) for magnetic virus complexes as compared to the virus alone across the whole tested range of nanomaterial-to-virus-particle ratios ($p < 0.05$ at 2 and 4 days postinfection and $p \leq 0.01$ at 6 days postinfection). The IC_{50} is defined as the concentration of virus resulting in a 50% inhibition of the maximal cell growth, as determined by fitting the experimental dose−response curves to the logistic function, as shown in Figure 5D. The IC_{50} values of the magnetic virus complexes in a range of nanoparticle-to-viral-particle ratios from 0.625 to 20 fg of Fe/VP were not significantly different. In addition, the oncolysis kinetics of the complexes was greatly improved when compared with the virus alone (Figure 5C). The IC_{50} of the virus alone dropped in an approximately linear manner over 6 days, while the oncolytic effect had fully developed within 48 h for magnetic complexes with magnetic-particle-to-virus ratios equal to or higher than 1.25 fg of Fe/VP. The fast kinetics of oncolysis was likely due to an early onset of virus replication because unspecific cytotoxicity, assessed in a control experiment with nonreplicating recombinant adenovirus, was only apparent at the highest nanoparticle-to-virus-particle ratio (40 fg of Fe/VP) with high virus doses (shown in Figure 5B). In the absence of a magnetic field, the IC_{50} values of the magnetic complexes were similar to virus alone except at high nanoparticle-to-virus particle ratios (10−40 fg of Fe/VP), where IC_{50} values were 1.4- to 2-fold higher, indicating a lower oncolytic effect (Table 3). The differences were statistically significant ($p \leq 0.014$). This inhibition of virus potency is likely due to compromised intracellular processing at excess magnetic particles but not due to a decrease in cellular uptake because the amount of internalized virus particles per cell at MOIs of 20 and 40 for complexes formulated at a ratio of 40 fg of Fe/VP was determined to be twice ($p < 0.05$) that for the uptake of the complexes at a ratio of 5 fg of Fe/VP (Figure S4 in the Supporting Information). Some decrease in oncolytic effect was also observed at excess of MNPs with high virus doses of 20 and 40 MOIs and high nanoparticle-to-viral-particle ratios of 40 fg of Fe/VP (Figure 6A). Overall, the 5 fg of Fe/VP composition turned out most useful for Ad520−PEI-Mag2 complexes upon magnetic field application because it combined high oncolytic potency and favorable biophysical characteristics with a relatively low concentration of magnetic particles.

Virus Uptake and Selective Oncolytic Effect of Magnetic Ad520 in Multidrug-Resistant 181RDB-fLuc Cells. For these experiments, multidrug-resistant (MDR) 181RDB-fLuc cells (6% of cells were positive for CAR) and drug-sensitive parental HeLa cells (HeLa-P; 98% of cells were CAR positive) were used as target cells and nontarget cells, respectively. Figure 6B demonstrates that the internalization of virus particles per cell with Ad520−PEI-Mag2

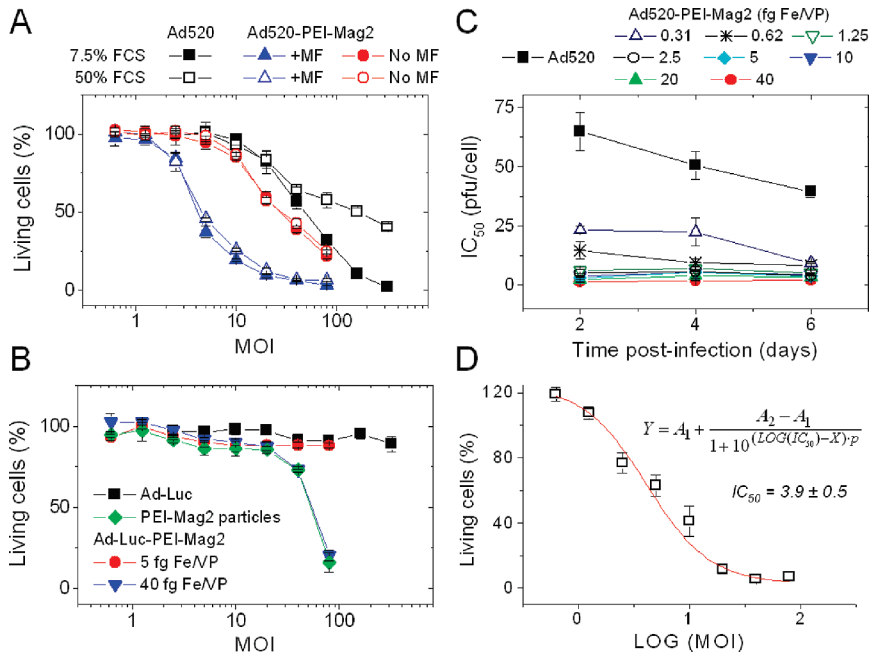

Figure 5. (A) Dose−oncolytic effect at 7.5% and 50% FCS in CAR-deficient multidrug-resistant 181RDB-fLuc cells. The cells were infected with either oncolytic adenovirus Ad520 or Ad520−PEI-Mag2 complexes in cell culture medium containing 7.5% or 50% FCS with (+MF) or without (no MF) positioning on the magnetic plate for 30 min after adding the virus or magnetic complexes. At 24 h postinfection, the virus-containing medium was replaced with fresh cell culture medium. Cell survival was assessed 6 days postinfection by a luciferase assay in cell lysates. The Ad520−PEI-Mag2 complexes were prepared in OptiMEM medium at a nanoparticle-to-viral particle ratio of 5 fg of Fe/VP. (B) Toxicity of Ad-Luc and Ad-Luc−PEI-Mag2 complexes in 181RDB-fLuc cells. Cell survival 6 days postinfection with nonreplicating E1-minus adenovirus expressing luciferase (Ad-Luc) alone or with its magnetic complexes prepared at 5 and 40 fg of Fe/VP or with PEI-Mag2 magnetic particles alone (magnetic particle concentration equivalent to the complexes formulated at 40 fg of Fe/VP) in cell culture medium containing 7.5% FCS. The plate was positioned on the magnetic plate for 30 min immediately after addition of the complexes. Cell survival was assessed by a MTT assay. (C) IC_{50} for the oncolysis of the 181RDB-fLuc cells with virus alone or with magnetic virus complexes prepared at different nanoparticle-to-virus particle ratios versus time postinfection in cell culture medium containing 7.5% FCS with positioning on the magnetic plate for 30 min after adding the virus or magnetic complexes. (D) Fitting of the experimental dose−response curve for the Ad520 magnetic complex (at 5 fg of Fe/VP, 6 days postinfection) to the logistic function.

Table 3. The Virus Concentrations That Inhibited 50% of the Maximal Cell Growth (IC_{50} in Terms of pfu/cell) of CAR-Deficient Multidrug-Resistant 181RDB-fLuc Cells at 2, 4, and 6 Days Postinfection[a]

	IC_{50}[b] (pfu/cell)			
nanoparticle-to-virus ratio (fg of Fe/VP)	2 days (+MF)	4 days (+MF)	6 days (+MF)	6 days (no MF)
0	64.8 ± 8.0	50.5 ± 5.9	39.4 ± 2.4	43.3 ± 4.8
0.3125	23.4 ± 1.7	22.5 ± 5.9	9.3 ± 0.3	42.5 ± 5.7
0.625	14.7 ± 3.7	9.5 ± 1.5	8.4 ± 1.9	43.7 ± 9.8
1.25	6.3 ± 1.3	7.0 ± 0.6	5.2 ± 0.2	39.3 ± 6.0
2.5	5.4 ± 1.4	5.7 ± 0.2	4.2 ± 0.4	38.7 ± 5.9
5	3.1 ± 0.5	5.5 ± 0.5	3.9 ± 0.5	36.6 ± 3.4
10	3.9 ± 0.5	5.4 ± 1.2	4.5 ± 0.6	88.0 ± 2.9
20	2.4 ± 0.8	4.0 ± 1.1	3.5 ± 0.8	92.6 ± 5.7
40	1.3 ± 0.2	1.9 ± 0.1	2.2 ± 0.3	62.1 ± 1.2

[a] Infection was performed in cell culture medium containing 7.5% FCS either with (+MF) or without (no MF) magnetic field application using Ad520 oncolytic adenovirus and its magnetic complexes with PEI-Mag2 nanoparticles prepared at different nanoparticle-to-virus ratios. [b] Mean ± SD ($n = 3$).

complexes in an applied magnetic field was 9- to 10-fold higher ($p < 0.05$) as compared to virus alone in both cell lines. The virus uptake in both cell lines was generally not significantly different despite the difference in CAR expression, which suggests that uptake was independent of the CAR expression status of these cells.

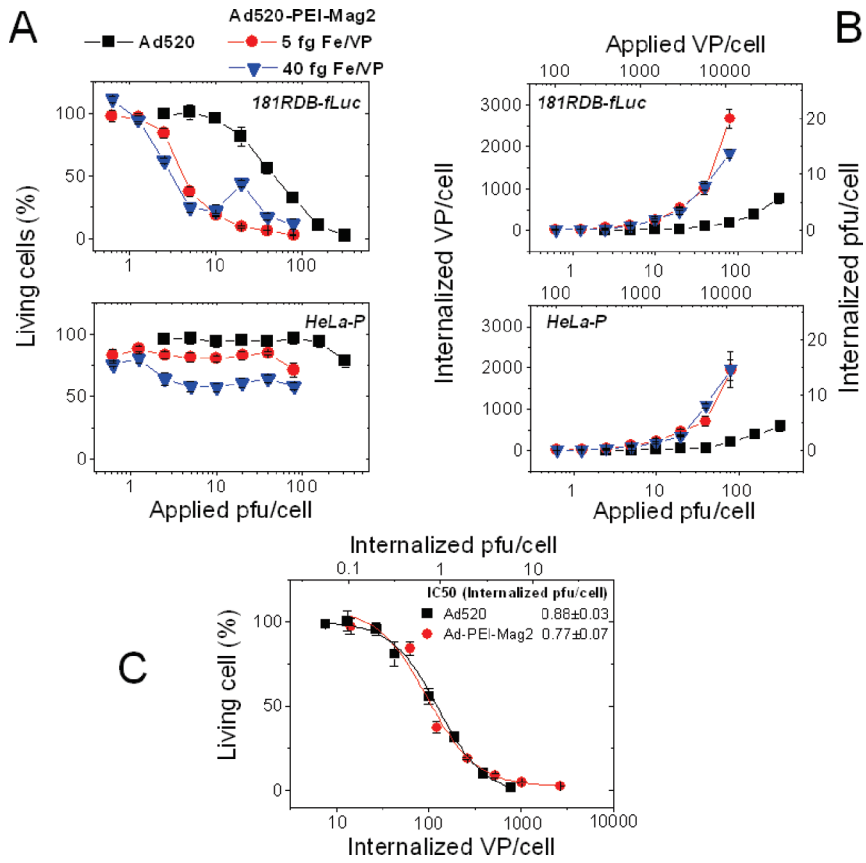

Figure 6. Virus internalization and the selective oncolytic effect of adenovirus Ad520 and its magnetic complexes with PEI-Mag2 magnetic nanoparticles for multidrug-resistant 181RDB-fLuc cells versus applied virus dose or internalized virus dose. (A) 181RDB-fLuc and HeLa-P cells were infected with oncolytic adenovirus Ad520 alone or with Ad520−PEI-Mag2 in cell culture medium containing 7.5% FCS with incubation at the magnetic plate for 30 min after addition of the virus or its magnetic complexes prepared at ratios of 5 and 40 fg of Fe/VP. Survival of the infected cells was evaluated with a luciferase assay in the cell lysates for 181RDB-fLuc cells and a MTT-based assay for HeLa-P cells 6 days postinfection. (B) Cells were infected with I^{125}-labeled virus or its magnetic complexes. Six hours postinfection, the cells were washed with PBS and then incubated with heparin solution, and cell-associated radioactivity was measured in the cell lysates. (C) Experimental data on the oncolytic effect of Ad520 or Ad520−PEI-Mag2 complexes at a ratio of 5 fg of Fe/VP in 181RDB-fLuc cells (shown in Figure 6A) were plotted against the internalized virus dose assessed from the experimental curves on virus internalization shown in Figure 6B. IC_{50} was calculated in terms of the internalized pfu/cell for both the virus and its magnetic complexes.

Despite similar uptake, we observed a pronounced dose-dependent oncolytic effect of Ad520 and its magnetic complexes only in the MDR target cells, not in HeLa-P cells (Figure 6A). In addition, the oncolytic potency of Ad520 as well as its magnetic complexes in MDR target cells was comparable to that of positive controls (wild-type adenovirus and its magnetic complexes, Figure S5A in the Supporting Information). In contrast, the wild-type adenovirus was nonspecifically capable of killing both MDR cells and HeLa-P cells (Figure S5B in the Supporting Information). Some of the effect observed for Ad520 complexes at the high magnetic particle-to-virus ratio of 40 fg of Fe/VP in HeLa-P cells can be attributed to nonspecific cytotoxicity, as was evident from a control experiment with nonreplicating recombinant adenovirus at the highest nanoparticle-to-virus particle ratio with high virus doses (Figure S6 in the Supporting Information). In contrast to oncolysis, the infectivity of magnetic adenovirus complexes, determined by a luciferase reporter gene expression, upon transduction with nonreplicating adenovirus expressing luciferase (Ad-Luc) magnetic complexes was very similar in both cell lines (Figure S7 in the Supporting Information). The highest infectivity was observed with the Ad-Luc−PEI-Mag2 complexes formulated at 5 fg of Fe/VP, similar to the highest oncolytic potency of the Ad520 magnetic complexes, which was also observed at this ratio.

To clarify whether the virus association with MNPs modulates the oncolytic activity of the virus, cell survival was plotted against the internalized virus dose for Ad520 alone and its magnetic complex. The resulting two nearly identical curves, which have very similar IC_{50} values (0.88 ± 0.03 internalized pfu/cell for Ad520 and 0.77 ± 0.07 internalized pfu/cell for its magnetic complex), are shown in Figure 6C. Hence, the virus association with MNPs did not inhibit the oncolytic activity of the virus, and the boost in oncolytic potential by magnetic force was correlated with

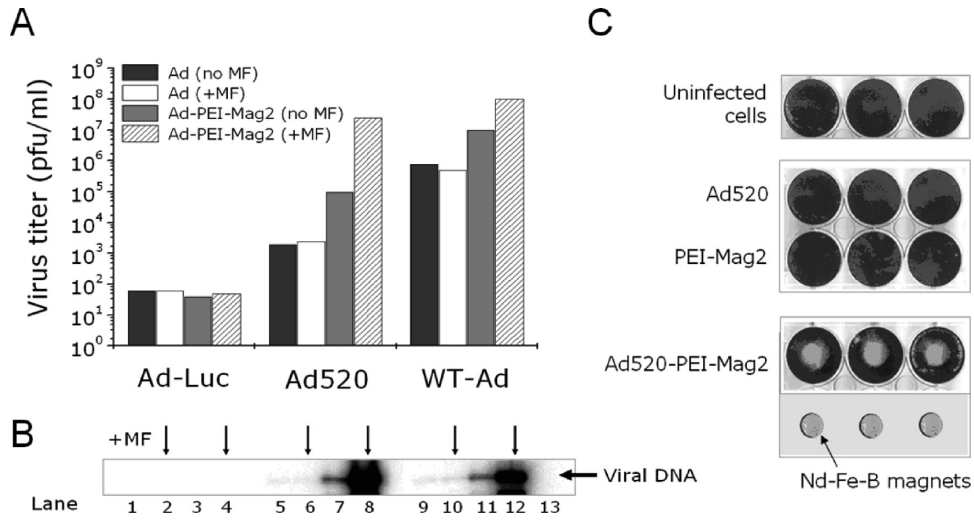

Figure 7. Viral particle production and viral DNA replication in CAR-deficient multidrug-resistant 181RDB cells after infection with oncolytic adenovirus Ad520 and Ad520−PEI-Mag2 complexes. 181RDB cells were infected with adenovirus Ad-Luc (negative control), Ad520, WT-Ad (positive control), or their complexes with PEI-Mag2 particles (Ad−PEI-Mag2) in 6-well plates. Virus particle concentration was 1.32×10^8 VP/well/2 mL/1.5×10^5 cells (MOI = 10), and the magnetic-nanoparticle-to-viral-particle ratio was 5 fg of Fe/VP. After 15 min incubation with (+MF) or without (no MF) magnetic field application, the infection medium was replaced with fresh cell culture medium. (A) Virus yields were measured by an end-point dilution assay on 293 cells 5 days postinfection, and (B) total purified DNA isolated from adenovirus-infected cells 3 days postinfection was digested with *Kpn*I and separated on 1% agarose gel. Southern blot analysis was performed using a specific E2A-cDNA probe. Lanes 1, 5, 9 and 2, 6, 10: after infection, with virus alone, without and with (marked with arrows) a magnetic field applied, respectively, for Ad-Luc, Ad520, and WT-Ad as shown in the figure. Lanes 3, 7, 11 and 4, 8, 12: after infection, with Ad−PEI-Mag2 complexes, without and with a magnetic field applied, respectively, for Ad-Luc, Ad520, and WT-Ad as shown in the figure. Lane 13: a control probe isolated from uninfected cells. (C) Targeted oncolytic effect of Ad520−PEI-Mag2 complexes. The 181RDB cells were infected with Ad520−PEI-Mag2 complexes or with Ad520 alone under magnetic field application for 15 min immediately after adding the complexes, followed by replacing the infection medium with fresh culture medium. Upon incubation with infection medium, the magnetic field was created by an array of 6 disk-shaped Nd−Fe−B magnets shown in the figure. Uninfected cells and PEI-Mag2 nanoparticles were used as negative controls. At 6 days postinfection, surviving cells were stained with sulforhodamine B.

the increase in virus uptake and was not caused by heightened oncolytic productivity per virus particle. Additionally, the oncolytic effect of magnetic virus complexes can be confined to an area under magnetic field influence, as shown in Figure 7C for MDR cells; no oncolytic effect was observed in the cells infected with Ad520 alone or with magnetic complexes without magnetic field application.

Virus Particle Production and Viral Replication upon Infection with Ad520−PEI-Mag2 in MDR Cells. The oncolytic activity of Ad520 is dependent on the ability of the virus to replicate and, in this way, induce cytopathic changes.[2] Therefore, we tested the ability of the nonreplicating control virus Ad-Luc (as a negative control), Ad520, and a replication-competent wild-type adenovirus (WT-Ad, as a positive control) to replicate and produce progeny virus particles in 181RDB cells and compared their abilities with their magnetic complexes. Figures 7A and 7B show that replication of Ad520 (lanes 5 and 6) and progeny virus particle production were lower than those of WT-Ad (lanes 9 and 10). Both viral DNA replication and virus particle production of Ad520 associated with PEI-Mag2 nanoparticles upon magnetic field application (lane 8) were considerably enhanced compared to both the virus alone (lanes 5 and 6) and the complexes with no field application (lane 7) but were comparable to those of WT-Ad magnetic complex (lane 12). Hence, the virus association with magnetic nanoparticles and application of the magnetic field could boost the amount of replicated viral DNA and the virus progeny production of Ad520.

Tumor Growth Inhibition upon Intratumoral Injection of Ad520 Magnetic Complexes in a Murine Xenograft Model. Based on the considerable enhancement of the oncolytic activity of Ad520 magnetic complexes compared to the Ad520 alone in MDR cells in vitro, we performed a pilot experiment to evaluate the effect of local intratumoral (i.t.) injection of magnetic Ad520 complexes in mouse tumor xenografts from human pancreatic carcinoma cells stably expressing firefly luciferase. The treatment schedule included three i.t. injections of PBS (control), Ad520 alone or Ad520−PEI-Mag2 magnetic complexes at days 0, 7, and 11 of treatment. No body weight loss was observed during the treatment. Tumor growth was evaluated by calculating the tumor volumes from measurements with a caliper and in addition by measuring firefly luciferase expression using an in vivo imaging system.

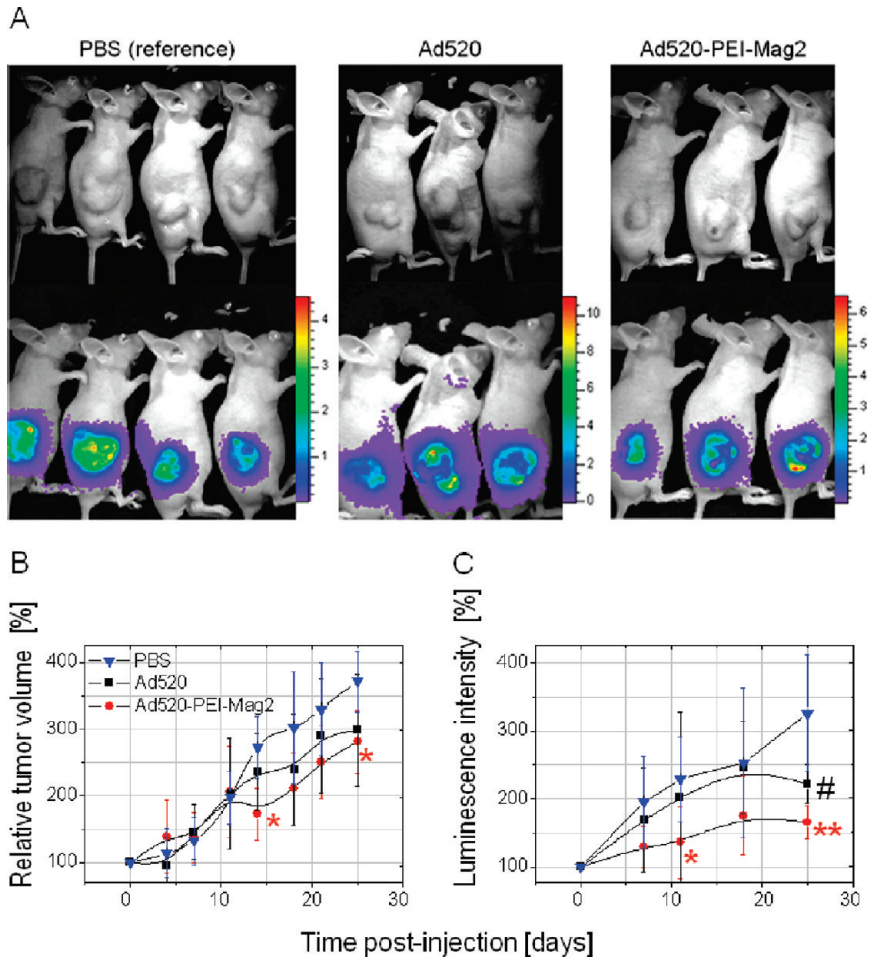

Figure 8. Growth of tumor xenografts in nude mice following intratumoral injection of PBS, Ad520 or Ad520−PEI-Mag2 magnetic complexes. (A) Representative white light and luminescence images of nude mice bearing tumor xenografts grown upon by subcutaneous injection of daunorubicin-resistant human pancreatic carcinoma cells stably expressing firefly luciferase. The images were taken at day 25 of treatment with PBS (left panel), Ad520 (middle panel) or Ad520−PEI-Mag2 magnetic complexes (right panel) as described in the Experimental Section. The scale for the luminescence images represents luminescence intensity in 10^9 photons/s/cm^2/steradian. (B) Tumor volume and (C) integral luminescence photon counts derived from the in vivo images as shown in panel A normalized to the values measured at day 0 of treatment. Data in graphs B and C are given as mean ± SD; * and ** indicate significant differences between Ad520−PEI-Mag2 and reference (PBS) groups with $p < 0.05$ and $p < 0.01$, respectively. # indicates significant differences between Ad520−PEI-Mag2 and Ad520 groups with $p < 0.05$.

According to the measurements of tumor volume, there was only a 20% inhibition of tumor growth by day 25 compared to PBS control upon treatment with Ad520 alone. The effect was not statistically significant. The treatment with Ad520−PEI-Mag2 magnetic complexes under magnetic field influence inhibited tumor growth statistically significantly compared to PBS control (Figure 8B). According to tumor volume measurements, the growth inhibition was 37% ($p = 0.01$) at day 14 and 25% by day 25 ($p = 0.02$).

The evaluation of tumor growth inhibition by bioluminescence in vivo imaging is shown in Figures 8A and 8C. Upon treatment with Ad520 alone, tumor growth was inhibited by 32% compared with PBS control (no statistical significance). The treatment with Ad520−PEI-Mag2 magnetic complexes under magnetic field influence resulted in statistically significant 41% inhibition by day 11 ($p = 0.049$) and 49% inhibition by day 25 ($p = 0.009$), respectively, compared with PBS control. Furthermore, by day 25, the difference of growth inhibition was also statistically significant compared with the Ad520 alone treatment ($p = 0.039$). In addition, whereas a decrease in imaging signal was measured between days 18 and 25, an increase in tumor volume was observed. This is in line with published observations on the higher significance of imaging techniques to evaluate the tumor growth inhibition.[9,56,57]

Regular PCR, specific for the adenovirus hexon gene performed on DNA extracts from tissues taken at day 25 of treatment, detected virus in the tumors of Ad520 treated animals but not in their livers (Figures 9A and 9B). As the liver is the primary organ of adenovirus tropism in mice, this result indicates that adenovirus replication was specific for the tumor tissue or that there was no spillover to other

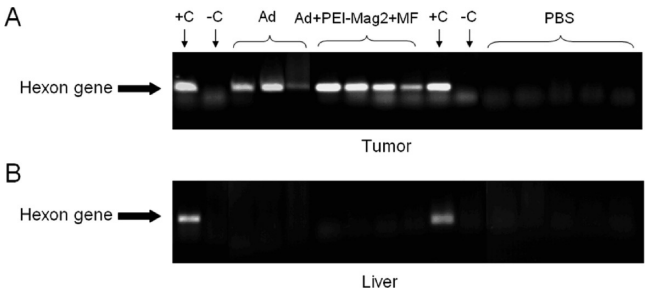

Figure 9. Viral DNA replication in tumor and liver samples of nude mice bearing tumor xenografts detected at day 25 of treatment by intratumoral injection of the Ad520−PEI-Mag2 magnetic complexes or only adenovirus Ad520 as described in the Experimental Section. Hexon gene detected by regular PCR in (A) tumor and (B) liver tissues of mice. The purified DNA isolated from an Ad520 preparation and DNA isolated from tumor or liver samples from a mouse of the control group (PBS treatment) were used as positive (+C) and negative controls (−C), respectively.

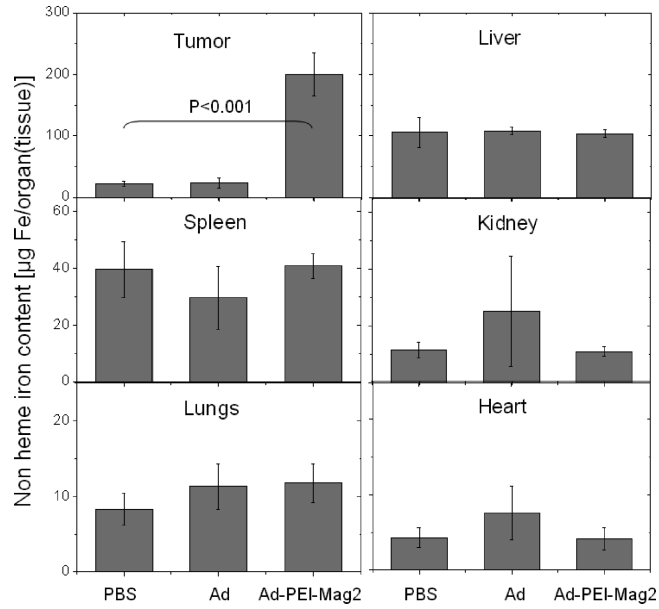

Figure 10. Non-heme iron content (mean ± SD) in tissues of mice at day 25 of treatment by intratumoral injection of the Ad520 magnetic complexes (Ad520−PEI-Mag2 group) or only Ad520 adenovirus (Ad group) as described in the Experimental Section. Tissue samples from the control group (PBS treatment) served as references.

organs at all. Non-heme iron analysis of isolated tissues detected magnetic nanoparticles only in the tumors and amounted to 200 ± 35 μg of exogenic iron (Figure 10). This matches almost exactly the injected dose of 201 μg, indicating that also the magnetic nanoparticles remained localized in the tumors.

Discussion

In this study, core−shell magnetite nanoparticles PEI-Mag2 were synthesized and self-assembled with the oncolytic adenovirus Ad520 by electrostatic interactions to enhance the oncolytic adenovirus potency under magnetic field-guided infection. The Ad520−PEI-Mag2 complexes can be formulated both in OptiMEM and in PBS with high virus binding capacity and stability even in the presence of high serum protein concentrations (Figure 2). The size and zeta potential measurements indicate that complex formation is robust and relatively insensitive toward the choice of media or virus concentration during complex assembly (Table 2 and Figure 2). The magnetic moments of the complexes calculated from their average velocities in a magnetophoretic mobility assay allow us to calculate an estimate of the MNP-to-virus ratio in the complex. The calculated 3,600 to 4,500 MNPs per virus particle for the optimized complex composition and the measured hydrodynamic diameter of 200 nm suggest that 3−4 layers of densely packed magnetite crystallites are arranged around a virus particle due to electrostatic interactions and possibly due to magnetic dipole−dipole interactions between the magnetic particles. Both AFM and TEM images confirm that the adenovirus was associated with PEI-Mag2 nanoparticles (Figure 4). The structural integrity of the virus was not impaired by its association with MNPs. Taken together, the magnetophoretic mobility measurements, particle sizing, AFM and TEM suggest a model where multiple layers of magnetite crystallites are associated with virus particles and where several virus particles can be linked by MNPs.

The oncolytic effect postinfection in culture media containing either 7.5% or 50% FCS was studied to reveal the influence of the observed opsonization of the virus and complexes, which results in a change of zeta potential (Table 2) and partial destabilization of the complexes (Figures 2A and 2D, Figure S2 in Supporting Information). In addition, infection in the presence of FCS better reflects the situation in vivo. High serum protein resistance was evidently observed in Ad520−PEI-Mag2 complexes but not for the virus alone (Figure 5A). Furthermore, the association of the virus with PEI-Mag2 nanoparticles did not interfere with the oncolytic activity but rather had a slight enhancing effect even without magnetic field application (Figure 5A). A 10-fold enhanced oncolytic activity in terms of the IC_{50} that developed very fast (Figure 5C and Table 3) was achieved when infections were carried out with magnetic virus complexes under magnetic field influence. This "enabling" effect is based on the 10-fold improved virus uptake (Figure

(56) Choi, H.; Charnsangavej, C.; Faria, S. C.; Macapinlac, H. A.; Burgess, M. A.; Patel, S. R.; Chen, L. L.; Podoloff, D. A.; Benjamin, R. S. Correlation of computed tomography and positron emission tomography in patients with metastatic gastrointestinal stromal tumor treated at a single institution with imatinib mesylate: proposal of new computed tomography response criteria. *J. Clin. Oncol.* **2007**, *25* (13), 1753–9.

(57) Van den Abbeele, A. D. The lessons of GIST--PET and PET/CT: a new paradigm for imaging. *Oncologist* **2008**, *13* (Suppl. 2), 8–13.

6) which resulted in 4 orders of magnitude higher virus progeny formation (Figure 7) compared to standard infection with Ad520 alone. In this respect one might expect an even stronger reduction of the IC_{50}. However, one should not forget that only the primary cycle of viral infection benefits from the enhancing effect of magnetofection by virtue of increased viral uptake. The observed virus uptake was independent of the CAR expression of cells (Figure 6). This observation is in agreement with the results of others who have described CAR-independent uptake pathways.[58−60] Smith et al. have demonstrated that CAR binding is not the major determinant of Ad5 virus tropism in vivo.[8] In contrast, integrins and heparan sulfate glycosaminoglycans play a significant role in vector delivery to the spleen, lungs and kidneys in nonhuman primates as well as in mice.[8] Furthermeore, the complexes of the virus with the positively charged PEI-Mag2 nanoparticles have a net positive zeta potential when assembled in OptiMEM or PBS at MNP-to-virus particle ratio higher than 1.25 fg of Fe/VP. Cationic magnetic nanoparticles were shown to enter into cells with high effectiveness[61] compared to neutral particles or slightly charged particles. Hence, the charge of the MNP−viral complexes can be a factor contributing to the enhanced internalization of the virus associated with magnetic nanoparticles. Decoration of the particles and thus of the whole complex with PEI can also contribute to the enhanced infectivity of the complexes with account for the high buffering capacity of PEI, especially at the slightly acid pH that is found in the endosomal vesicles. The PEI proton sponge effect is thought to decrease trafficking of the complexes to degradative lysosomes.[62]

The specific oncolytic effect of Ad520 magnetic complexes in MDR cells (Figure 7) indicates that the intrinsic biological properties of the virus remained unchanged upon association with MNPs and that the target cell specificity of Ad520 examined here is not governed by uptake but by downstream intracellular events resulting in specific replication in MDR cells. The advantage of the magnetofection method is not only the enhanced virus uptake and oncolytic potency but also targeting the oncolytic effect of magnetic virus complexes to a specific area where the magnetic field was positioned (Figure 7C).

A pilot experiment in a tumor xenograft model in mice revealed improved tumor growth retardation upon intratumoral injection of magnetic Ad520 complexes under magnetic field influence versus virus alone (Figure 8). Moreover, both adenovirus and MNPs of the complexes remained localized only in the tumor xenograft (Figures 9 and 10). To evaluate tumor growth retardation, we chose the classical caliper measurements and in addition bioluminescence measurements. The reason is that recent studies have shown that some agents induce tumor necrosis without affecting the apparent dimensions of tumors.[9] Therefore, new criteria for detecting the response to treatment by imaging are evaluated.[56,57] It is known that the penetration of oncolytic adenoviruses through the tumor mass is limited upon intratumoral injection.[63] Hence the determination of the apparent tumor volume may lead to an underestimation of the oncolytic activity. In fact, in our experiments the evaluation of tumor growth by luminescence imaging indicated a substantially stronger growth inhibition than apparent from the determination of the tumor volumes. Based on the data from the pilot experiment we cannot exclude that the magnetic nanoparticles contributed an additional cytotoxic effect. The fact that we did not observe complete tumor remissions indicates that intratumoral magnetofection with an oncolytic adenovirus cannot overcome all limitations inherent in the virus. We assume that the significantly superior tumor growth retardation observed with the magnetic complexes of Ad520 can be attributed to enhanced virus uptake into tumor cells during the magnetically assisted first round of infection. But magnetofection can impossibly enhance subsequent infection cycles by virus progeny which would proceed at the lower infectivity of the nonmagnetic virus. Nevertheless, one can expect a substantial impact of the magnetic enhancement for viruses which are armed with functionality for improved tumor penetration[64] or other transgenes or treatments that mediate added direct or indirect antitumoral activity.

While this study has been focused on generating a nanomagnetic formulation of an oncolytic adenovirus in order to boost its tumor-specific cytotoxic potency, the greater context of progress in bionanotechnology and nanomedicine highlights potential implications of this work. Current efforts are dedicated to generating multifunctional nanoparticles or formulations of active agents that comprise modules for tissue targeting, for specific uptake and programmed intracellular processing in target cells and for noninvasive detection.

(58) Damm, E. M.; Pelkmans, L.; Kartenbeck, J.; Mezzacasa, A.; Kurzchalia, T.; Helenius, A. Clathrin- and caveolin-1-independent endocytosis: entry of simian virus 40 into cells devoid of caveolae. *J. Cell Biol.* **2005**, *168* (3), 477–88.

(59) Medina-Kauwe, L. K. Endocytosis of adenovirus and adenovirus capsid proteins. *Adv. Drug Delivery Rev.* **2003**, *55* (11), 1485–96.

(60) Shimony, N.; Elkin, G.; Kolodkin-Gal, D.; Krasny, L.; Urieli-Shoval, S.; Haviv, Y. S. Analysis of adenoviral attachment to human platelets. *Virol. J.* **2009**, *6*, 25.

(61) Villanueva, A.; Canete, M.; Roca, A. G.; Calero, M.; Veintemillas-Verdaguer, S.; Serna, C. J.; Morales Mdel, P.; Miranda, R. The influence of surface functionalization on the enhanced internalization of magnetic nanoparticles in cancer cells. *Nanotechnology* **2009**, *20* (11), 115103.

(62) Sonawane, N. D.; Szoka, F. C., Jr.; Verkman, A. S. Chloride accumulation and swelling in endosomes enhances DNA transfer by polyamine-DNA polyplexes. *J. Biol. Chem.* **2003**, *278* (45), 44826–31.

(63) Kim, J. H.; Lee, Y. S.; Kim, H.; Huang, J. H.; Yoon, A. R.; Yun, C. O. Relaxin expression from tumor-targeting adenoviruses and its intratumoral spread, apoptosis induction, and efficacy. *J. Natl. Cancer Inst.* **2006**, *98* (20), 1482–93.

(64) Ganesh, S.; Gonzalez Edick, M.; Idamakanti, N.; Abramova, M.; Vanroey, M.; Robinson, M.; Yun, C. O.; Jooss, K. Relaxin-expressing, fiber chimeric oncolytic adenovirus prolongs survival of tumor-bearing mice. *Cancer Res.* **2007**, *67* (9), 4399–407.

Theranostics is the vision of combining therapy and diagnosis. Nanomagnetic compositions can serve both purposes.[65] They provide the opportunity of combining physical targeting by magnetic force with biological targeting,[66] have been used for inducing local hyperthermia,[67] have been used as drug carriers in clinical studies,[68] can be equipped with moieties for multimodal imaging[69] and are approved contrast agents for magnetic resonance imaging (MRI). MRI relaxometry has been used to detect adenovirus in biological media with high sensitivity and can be used to determine the assembly status of viral magnetic compositions.[70] With respect to preparing such compositions, much can be learned from recent work on using specifically adenoviruses as building blocks for generating targeted nanomagnetic theranostics.[32,71−73]

Apart from using armed oncolytic adenoviruses as therapeutic agents, we envisage two strategies where nanomagnetic targeting and enhancement of cellular uptake can lead to improved efficacy. One is employing infected carrier cells as tumor-homing therapeutic agents.[12−14] The in vitro transduction step which is required to prepare such cells certainly can be enhanced by nanomagnetic means. But based on recent literature, also the accumulation of such cells in tumors probably can be enhanced by magnetic force[21,74,75] and the process can be monitored by MRI.[74,75] The other strategy for a nanomagnetic enhancement of oncolytic adenovirotherapy is upon intravascular administration. For this purpose, one would prepare biologically targeted and shielded magnetic virus compositions, similarly as described for example by Morrison or by Kreppel and colleagues for nonmagnetic adenovirus.[11,76] Administration into a tumor-feeding blood vessel would provide the opportunity to exploit the enhanced permeability and retention effect to result in more uniform coverage of the tumor tissue than intratumoral injection. The applied magnetic force not only would serve for accumulation purposes but also would boost the first-round infection efficiency as demonstrated in our in vitro and in vivo experiments. This would result in a greater progeny population that was more evenly distributed throughout the tumor and inherently armed for further efficient infection cycles.

Conclusions

We conclude that magnetic targeting of virus particles decorated with suitable magnetic nanoparticles can, in fact, enable the inherent potency of an oncolytic adenovirus analogous to the classical magnetic targeting of cytostatic drugs, which exploits their inherent potencies without altering their inherent mechanisms of action. However, the full effect in a real tumor will require a combination of molecular biological and chemical strategies, specifically targeting, arming and shielding. Recent progress in bionanotechnology provides multiple opportunities to equip oncolytic viruses with additional functions and to enhance their efficacies.

Acknowledgment. Financial support from the Thailand Research Fund (TRF) through the Royal Golden Jubilee Ph.D. programme (Grant No. PHD/0002/2548) is gratefully acknowledged. Support was also obtained by Deutsche Forschungsgemeinschaft DFG (Project PL 281/3-1).

Supporting Information Available: Additional experimental details and figures as discussed in the text. This material is available free of charge via the Internet at http://pubs.acs.org.

MP100123T

(65) Veiseh, O.; Gunn, J. W.; Zhang, M. Design and fabrication of magnetic nanoparticles for targeted drug delivery and imaging. *Adv. Drug Delivery Rev.* **2010**, *62* (3), 284–304.

(66) Pradhan, P.; Giri, J.; Rieken, F.; Koch, C.; Mykhaylyk, O.; Doblinger, M.; Banerjee, R.; Bahadur, D.; Plank, C. Targeted temperature sensitive magnetic liposomes for thermo-chemotherapy. *J. Controlled Release* **2010**, *142* (1), 108–21.

(67) Thiesen, B.; Jordan, A. Clinical applications of magnetic nanoparticles for hyperthermia. *Int. J. Hyperthermia* **2008**, *24* (6), 467–74.

(68) Lubbe, A. S.; Alexiou, C.; Bergemann, C. Clinical applications of magnetic drug targeting. *J. Surg. Res.* **2001**, *95* (2), 200–6.

(69) Medarova, Z.; Pham, W.; Farrar, C.; Petkova, V.; Moore, A. In vivo imaging of siRNA delivery and silencing in tumors. *Nat. Med.* **2007**, *13* (3), 372–7.

(70) Perez, J. M.; Simeone, F. J.; Saeki, Y.; Josephson, L.; Weissleder, R. Viral-induced self-assembly of magnetic nanoparticles allows the detection of viral particles in biological media. *J. Am. Chem. Soc.* **2003**, *125* (34), 10192–3.

(71) Manchester, M.; Singh, P. Virus-based nanoparticles (VNPs): platform technologies for diagnostic imaging. *Adv. Drug Delivery Rev.* **2006**, *58* (14), 1505–22.

(72) Saini, V.; Martyshkin, D. V.; Mirov, S. B.; Perez, A.; Perkins, G.; Ellisman, M. H.; Towner, V. D.; Wu, H.; Pereboeva, L.; Borovjagin, A.; Curiel, D. T.; Everts, M. An adenoviral platform for selective self-assembly and targeted delivery of nanoparticles. *Small* **2008**, *4* (2), 262–9.

(73) Singh, R.; Kostarelos, K. Designer adenoviruses for nanomedicine and nanodiagnostics. *Trends Biotechnol.* **2009**, *27* (4), 220–9.

(74) Loebinger, M. R.; Kyrtatos, P. G.; Turmaine, M.; Price, A. N.; Pankhurst, Q.; Lythgoe, M. F.; Janes, S. M. Magnetic resonance imaging of mesenchymal stem cells homing to pulmonary metastases using biocompatible magnetic nanoparticles. *Cancer Res.* **2009**, *69* (23), 8862–7.

(75) Riegler, J.; Wells, J. A.; Kyrtatos, P. G.; Price, A. N.; Pankhurst, Q. A.; Lythgoe, M. F. Targeted magnetic delivery and tracking of cells using a magnetic resonance imaging system. *Biomaterials* **2010**, *31* (20), 5366–71.

(76) Kreppel, F.; Kochanek, S. Modification of adenovirus gene transfer vectors with synthetic polymers: a scientific review and technical guide. *Mol. Ther.* **2008**, *16* (1), 16–29.